Mineralogical Magazine, October 2017, Vol. 81(5), pp. 1165–1189

Fluorophlogopite-bearing and carbonate metamorphosed xenoliths from the Campanian Ignimbrite (Fiano, southern Italy): crystal chemical, geochemical and volcanological insights

M. Lacalamita[1], G. Balassone[2], E. Schingaro[1,*], E. Mesto[1], A. Mormone[3], M. Piochi[3], G. Ventruti[1] and M. Joachimski[4]

[1] Dipartimento di Scienze della Terra e Geoambientali, Università degli Studi di Bari Aldo Moro, via Orabona 4, I-70125 Bari, Italy
[2] Dipartimento di Scienze della Terra dell'Ambiente e delle Risorse, Università "Federico II", Complesso Universitario Monte S. Angelo, Via Cinthia, I-80126 Napoli, Italy
[3] Istituto Nazionale di Geofisica e Vulcanologia, Osservatorio Vesuviano, via Diocleziano 328, I-80124 Napoli, Italy
[4] GeoZentrum Nordbayern, Universität Erlangen-Nürnberg, Erlangen 91054, Germany

[*Received 27 December 2015; Accepted 2 October 2016; Associate Editor: Ed Grew*]

ABSTRACT

Fluorine-, boron- and magnesium-rich metamorphosed xenoliths occur in the Campanian Ignimbrite deposits at Fiano (southern Italy), at ~50 km northeast of the sourced volcanic area. These rocks originated from Mesozoic limestones of the Campanian Apennines, embedded in a fluid flow. The Fiano xenoliths studied consist of ten fluorophlogopite-bearing calc-silicate rocks and five carbonate xenoliths, characterized by combining mineralogical analyses with whole-rock and stable isotope data. The micaceous xenoliths are composed of abundant idiomorphic fluorophlogopite, widespread fluorite, F-rich chondrodite, fluoborite, diopside, Fe(Mg)-oxides, calcite, humite, K-bearing fluoro-richterite and grossular. Of the five mica-free xenoliths, two are calcite marbles, containing subordinate fluorite and hematite, and three are weakly metamorphosed carbonates, composed only of calcite. The crystal structure and composition of fluorophlogopite approach that of the end-member. The Fiano xenoliths are enriched in trace elements with respect to the primary limestones. Comparisons between the rare-earth element (*REE*) patterns of the Fiano xenoliths and those of both Campanian Ignimbrite and Somma-Vesuvius marble and carbonate xenoliths show that the Fiano pattern overlaps that of Somma-Vesuvius marble and carbonate xenoliths, and reproduces the trend of Campanian Ignimbrite rocks. Values of $\delta^{13}C$ and $\delta^{18}O$ depict the same trend of depletion in the heavy isotopes observed in the Somma-Vesuvius nodules, and is related to thermometamorphism. Trace-element distribution, paragenesis, stable isotope geochemistry and data modelling point to infiltration of steam enriched in F, B, Mg and As into carbonate rocks at a temperature of ~300–450°C during the emplacement of the Campanian Ignimbrite.

Keywords: Fiano xenoliths, Campanian Ignimbrite, Southern Italy, fluorophlogopite, crystal chemistry, geochemistry.

Introduction

Fluorine-, boron- and magnesium-rich metamorphosed xenoliths within the distal Campanian Ignimbrite deposits (Campania region, southern Italy) have attracted the interest of the scientific community since the nineteenth century for their unusual mineralogy and occurrence. Studies were generally devoted to the crystal chemistry of some of the rare minerals found in these rocks, such as fluoborite (Brisi and Eitel, 1957; Flamini *et al.*, 1979; Cámara and Ottolini, 2000), norbergite

*E-mail: emanuela.schingaro@uniba.it
https://doi.org/10.1180/minmag.2016.080.155

(White, 1981) and chondrodite (Balassone *et al.*, 2002). The parental rocks of these xenoliths are Mesozoic sedimentary carbonates of the Campanian Apennines. Carbonate fragments were embedded randomly in the pyroclastic flow during its travel to the surface and emplacement. Their interactions with hot and volatile-rich ignimbritic flow produced thermal metamorphic effects to a varying extent, although located far from the source volcanic area (e.g. the Phlegraean Fields; Fig. 1).

The distinctive characteristic of these xenoliths is the ubiquitous presence of later-formed fluorite and the occurrence of F-B-Mg-bearing mineral phases. They were found typically at Fiano, ~20 km northwest of Salerno, and east of the Phlegraean Fields (~50 km) and Somma-Vesuvius (~20 km), both active Campanian volcanoes (Fig. 1). Several quarries (the so-called 'Tufare') at Fiano were exploited intensively in the past for tuffaceous building materials, resulting in the recovery of xenoliths containing F-, B- and Mg-rich minerals (Carati, 1987). The 'Tufare' are currently inactive, because of the decreased demand for grey tuff as a building stone (de Gennaro *et al.*, 2013). Similar xenoliths have been described in the Campanian Ignimbrite exposed in the Caserta province (Scacchi, 1888, 1890; Zambonini, 1919; Carati, 1987), and in tuffs from the Colli Albani volcanic area of the Latium region (the 'Pozzolane nere' of Corcolle, near Tivoli: Bachechi *et al.*, 1966; Turi, 1969; Masi and Turi, 1972; Caponera *et al.*, 2003).

Although the Fiano xenoliths have received considerable amount of attention over the last 100 years (Scacchi, 1888, 1890; Zambonini, 1919; Masi and Turi, 1972; Carati, 1987), there has not yet been a thorough investigation using the latest developments in methodology and instrumentation. In the present study, xenoliths hosted in Campanian Ignimbrite pyroclastic deposits were investigated using combined mineralogical, geochemical and stable isotope analyses. Our results are compared with data from studies of carbonate xenoliths within the Somma-Vesuvius tephra (Barberi and Leoni, 1980; Del Moro *et al.*, 2001; Gilg *et al.*, 2001; Fulignati *et al.*, 2005), which also originated from the same Mesozoic sedimentary carbonates constituting the basement under the volcanoes. The results of this study allow an interpretation of the genetic subaerial environment of the xenoliths, and of their peculiar mineral assemblages, as well as the conditions during, and following, the deposition of the Campanian Ignimbrite.

Occurrence

Volcanological context

The Campania region hosts one of the most active volcanic complexes in Europe. Here, the Phlegraean Fields located near Naples (Fig. 1) represent a large cluster of alkaline volcanic vents, including the eponymous caldera (e.g. Vitale and Isaia, 2014; Piochi *et al.*, 2015). The Campanian Ignimbrite eruption dates to ~40 ka based on $^{40}Ar/^{39}Ar$ sanidine geochronology (Fedele *et al.*, 2008). Fallout products from this eruption occur over a wide area (from locations within the Tyrrhenian Sea to the Volga River in Russia and the Black Sea: see Giaccio *et al.*, 2008 and references therein), thus representing an important stratigraphic marker in palaeoclimate and archaeological studies (e.g. Fedele *et al.*, 2002; Costa *et al.*, 2012).

The Campanian Ignimbrite juvenile tephra range in composition from trachyte to phono-trachyte (Civetta *et al.*, 1997); are mostly glassy; and contain 3 to 10 vol.% of dominant sanidine and minor plagioclase, diopside, biotite, magnetite and apatite (Civetta *et al.*, 1997; Pappalardo *et al.*, 2008). Major, trace and Sr-isotope geochemistry suggest that these rocks originate from a normally stratified magma chamber with the uppermost phono-trachytic magma layer contaminated by hydrothermal fluids prior to eruption (Civetta *et al.*, 1997). On the basis of feldspar composition, the pre-eruptive temperature was estimated at 850 ± 40°C, lower than the homogenization temperature of 980°C estimated for melt inclusions within clinopyroxene at a pH_2O of 100–200 MPa (Piochi *et al.*, 2008 and references therein). Based on the variation of the volatile contents in melt inclusions trapped at different pressures, magma degassing during the ascent has been suggested (Marianelli *et al.*, 2006). As a result, the glassy groundmass in the juvenile fragments has a low H_2O content (0.3–0.6 wt.%) and F and Cl concentrations of ~0.26 and 0.78 wt.%, respectively (Signorelli *et al.*, 2001; Piochi *et al.*, 2008). The Cl content is in the range of variability found in the glassy matrix and in melt inclusions (from 0.34 to 0.89 wt.% in Marianelli *et al.*, 2006). Biotite has F contents between 0.7 and 2.5 wt.% and Cl concentrations between 0.04 and 0.14 wt.% in pumices (Civetta *et al.*, 1997), but has higher F contents (3.39–6.76 wt.%) in the syenite nodules in the proximal facies of the Campanian Ignimbrite (i.e. the 'Breccia Museo' deposit; Fedele *et al.*, 2006, 2008).

https://doi.org/10.1180/minmag.2016.080.155 Published online by Cambridge University Press

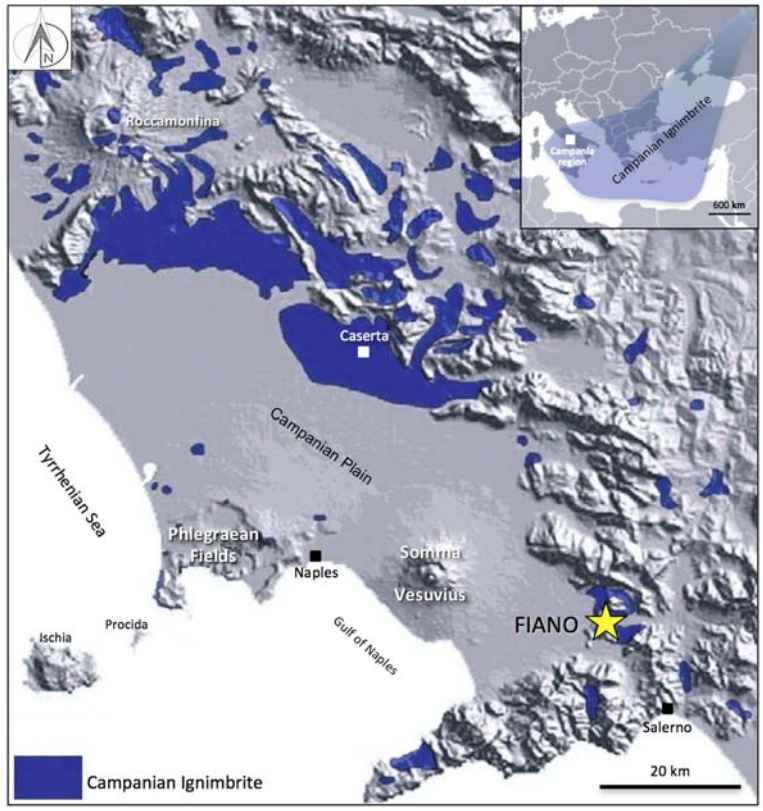

FIG. 1. Map of the Campania region, showing the extent of the Campanian Ignimbrite outcrops (modified after Arienzo *et al.*, 2011), as well as the Phlegraean and Somma-Vesuvius volcanic areas; the sampling location at Fiano is indicated by a yellow star. The top right inset illustrates the extent of the Campanian Ignimbrite tephra in south-eastern Europe within its limits of preservation (Fedele *et al.*, 2008).

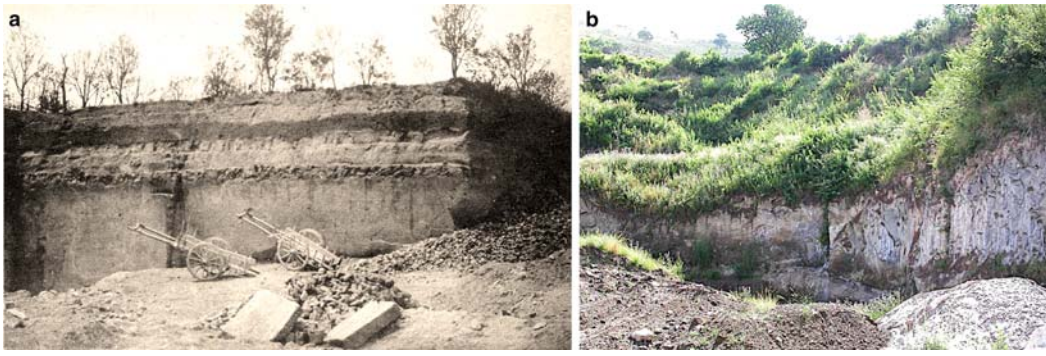

FIG. 2. (*a*) The Fiano quarries (the so called 'Tufare') for extraction of the Campanian Ignimbrite (Campanian Ignimbrite), as appeared at the beginning of the 20th century (after Zambonini, 1919). Grey tuff is at the base, overlaid by alternating layers of grey and yellow tuffs, with big limestone blocks. (*b*) Present day Campanian Ignimbrite outcrops, with the grey tuff showing the remains of the old mining activity (courtesy of P. Kastenmeier).

https://doi.org/10.1180/minmag.2016.080.155 Published online by Cambridge University Press

Grey and yellow lithified facies are recognized in the Campanian Ignimbrite. The grey facies is characterized by three lithologies with different textures: a basal part with a typical eutaxitic texture ('Piperno'), an intermediate part with weakly collapsed scoriae (pipernoid tuff) and an upper chaotic part (Langella *et al.*, 2013 and references therein). Feldspathization to various degrees of the grey facies and zeolitization of the yellow facies have been reported (Cappelletti *et al.*, 2003). The Campanian Ignimbrite exposed in the area studied (Fig. 2) can be related to magmas with a trachyphonolite composition, following Civetta *et al.* (1997). The exposure is represented mainly by the Welded Grey Ignimbrite with a thickness from a few metres to a few tens of metres (Langella *et al.*, 2013), generally composed of grey ash. It is poorly-sorted, massive, or showing inverse grading, and shows no traction-induced sedimentary structure. The lowermost massive part is white-to-cream in colour, relatively fine-grained, and contains sparse pumice lapilli and rare scoria lapilli towards the top. This part becomes gradually darker and grades upwards into a welded grey zone previously called the Grey Tuff, which is composed of rounded scoria lapilli, inversely graded black scoriae, embedded in an ashy matrix with subordinate xenoliths and crystals. Locally, this welded portion shows columnar jointing. At the top of the Welded Grey Ignimbrite, the degree of welding is minor with equant scoria fragments dispersed in an ashy matrix. Sub-vertical elutriation pipes are locally present at various heights. The Welded Grey Ignimbrite is overlaid locally by the Lithified Yellow Tuff, which consists of an ashy matrix with rounded lapilli to dispersed blocky pumice clasts. The uppermost incoherent unit consists of coarse pumice clasts within an ashy matrix (Langella *et al.*, 2013). In the Campania region, outcrops of the Campanian Ignimbrite are found typically overtopping the limestone mountains at altitudes up to 1000 m. They can also be the thickest outcrops in the valleys, as a result of the expanded (and therefore turbulent) pyroclastic current (Fisher *et al.*, 1993).

The xenoliths

The F-rich xenoliths within the Campanian Ignimbrite were first described by Scacchi (1890) and Zambonini (1919). The authors recognized many newly-formed phases, some of which subsequently discredited, like 'nocerite', 'grothine' and 'fluosiderite', synonyms of fluoborite, norbergite and chondrodite, respectively (Brisi and Eitel, 1957; White, 1981; Balassone *et al.*, 2002). The Fiano mineral assemblage is represented mainly by halides, F-, Mg- and Ca-bearing silicates, carbonates and oxides, with subordinate borates, arsenates and vanadates (Table 1). The xenoliths exhibit different dimensions, ranging from a few millimetres to several centimetres (Carati, 1987). An exceptional occurrence of a block of 2.3 m × 1.4 m × 0.7 m was described by Scacchi (1890). According to Carati (1987 and references therein), the xenoliths were grouped initially into 'micaceous

TABLE 1. An overall list of ideal crystal-chemical formulas of minerals found in the Fiano xenoliths, from both this study and the literature (Masi and Turi, 1972; Carati, 1987 and reference therein). Phases in italics are found in the samples investigated here.

Minerals	Ideal formulas*
aragonite, *calcite*	$CaCO_3$
augite	$(Ca,Na)(Mg,Fe,Al,Ti)(Si,Al)_2O_6$
biotite	$K(Mg,Fe^{2+})_3AlSi_3O_{10}(OH,F)_2$
chondrodite	$(Mg,Fe^{2+})_5(SiO_4)_2(F,OH)_2$
diopside	$CaMgSi_2O_6$
fluoborite	$Mg_3(BO_3)(F,OH)_3$
fluorite	CaF_2
fluorophlogopite	$KMg_3(AlSi_3)O_{10}F_2$
*fluoro-richterite***	$Na(NaCa)Mg_5[Si_8O_{22}]F_2$
grossular	$Ca_3Al_2(SiO_4)_3$
hematite	Fe_2O_3
hornblende	$Ca_2(Mg,Fe^{2+})_4(Al,Fe^{3+})Si_7AlO_{22}(OH)_2$
hörnesite	$Mg_3(AsO_4)_2{\cdot}8(H_2O)$
humite	$Mg_7(SiO_4)_3(F,OH)_2$
hydromagnesite	$Mg_5(CO_3)_4(OH)_2{\cdot}4(H_2O)$
*magnesioferrite***	$MgFe_2O_4$
magnetite	$Fe^{2+}Fe^{3+}_2O_4$
marialite	$Na_4Al_3Si_9O_{24}Cl$
microsommite	$(Na,Ca,K)_{7-8}(Si,Al)_{12}O_{24}(Cl,SO_4)_{2-3}$
norbergite	$Mg_3SiO_4F_2$
periclase	MgO
sanidine	$KAlSi_3O_8$
sellaite	MgF_2
spinel	$MgAl_2O_4$
vanadinite	$Pb_5(VO_4)_3Cl$
vonsenite	$Fe^{2+}_2Fe^{3+}O_2(BO_3)$

*From http://rruff.info/ima/#.
**Detected for the first time in the samples from this study.

https://doi.org/10.1180/minmag.2016.080.155 Published online by Cambridge University Press

clasts', 'fluoriferous geodes' and 'weakly metamorphosed carbonate rocks'. The micaceous xenoliths (1–35 cm in size) have friable mica-bearing crusts, brown to honey yellow in colour. These rocks were considered as derived from limestone protoliths, metamorphosed to a varying extent, and commonly characterized by one or more crusts and a nucleus constituted by calcite, as a relict of the primary limestone. Fluorite is widespread and pervasive; fluoborite and chondrodite are also common in the various coatings. The 'fluoriferous geodes' represent the final product of the metamorphic process affecting the limestone (Masi and Turi, 1972), and are composed mostly of microcrystalline fluorite and rare calcite. The 'weakly metamorphosed carbonate rocks' have variable dimensions, and can locally show fluorite-rich veinlets and voids and/or rare silicates as thin external coatings.

The fifteen xenoliths studied here originate from a private collection (Prof. E. Franco). They were sampled in the late 1980s at the top of the grey tuff at Fiano embedded in the Welded Grey Ignimbrite (Fig. 2), close to the so-called quarry "B" of Scacchi (1890). These rocks range from ~8–14 cm in size, and correspond to micaceous and carbonate xenoliths of the above mentioned literature. As shown in Table 2, and described in more detail below, mica-bearing xenoliths (ten samples) are prevalent over carbonate-dominated mica-free samples (five samples).

Analytical methods

The Fiano xenoliths were characterized mineralogically and petrographically by combining polarizing optical microscopy, powder X-ray diffraction (PXRD) and scanning electron microscopy equipped with an energy-dispersive spectrometer (SEM-EDS). PXRD was conducted using a Seifert-GE diffractometer ID 3003 (Dipartimento di Scienze della Terra, dell'Ambiente e delle Risorse, University of Naples Federico II, Italy). Intensity profiles were collected in the 2θ range of 3–80° using Ni-filtered Cu*K*α radiation (λ = 1.5406 Å) at 40 kV and 30 mA, with a step size 0.02°, at a scanning time of 10 s/step. The diffraction patterns were processed using the *RayfleX* software package. A minor set of measurements were performed by using an X'Pert Powder diffractometer by PANalytical (Istituto Nazionale di Geofisica e Vulcanologia Osservatorio Vesuviano, Naples, Italy), with a high speed PIXcel detector, Ni-filtered Cu*K*α radiation (λ = 1.5406 Å), at 40 kV and 40 mA in the 3–70°2θ range, with 0.02° steps at 8 s/step. Diffraction patterns were processed and interpreted using the PANalytical B.V. software *HIGHScore Plus* version 3.0e. The SEM examination was carried out using a JEOL JSM 5310 instrument at Dipartimento di Scienze della Terra, dell'Ambiente e delle Risorse, University of Naples, Italy. Element mapping in back-scattered electron mode (BSE) and EDS microanalyses were obtained with an INCA X-stream pulse processor and the 4.08 version *Inca* software (Oxford Instruments detector), interfaced with the JEOL JSM 5310. The following reference standards were used: albite (Si, Al, Na); orthoclase (K); wollastonite (Ca); diopside (Mg); almandine (Fe); rutile (Ti); barite (Ba); strontianite (Sr); metallic chromium (Cr); rhodonite (Mn); pyrite (S); sphalerite (Zn); galena (Pb); fluorite (F); apatite (P); sylvite (Cl); Smithsonian phosphates (La, Ce, Nd, Sm, Y); gallium arsenide (As); and metallic vanadium (V). Analytical errors are 1% relative for major elements and 3% relative for minor elements.

Ten xenoliths, including seven micaceous and three carbonate ones, were selected for whole-rock analysis, carried out at Bureau Laboratories Ltd. (Vancouver, Canada). Major elements were analysed by X-ray fluorescence (XRF) and inductively coupled plasma-emission spectrometry (ICP-ES), using $LiBO_2/Li_2B_4O_7$ fusion. Minor and trace elements were determined by inductively coupled plasma-mass spectrometry (ICP-MS), using a four-acid (HNO_3-$HClO_4$-HF-HCl) digestion. The uncertainty is <3% for major/minor oxides, <5–10% for trace elements. Loss on ignition (LOI) was calculated by weight loss after ignition at 1000°C.

Stable carbon and oxygen isotope analyses were carried out at the University of Erlangen-Nürnberg (Germany) on nine calcite-bearing samples (both carbonate and micaceous xenoliths). Carbonate powders (checked for impurities by powder diffraction) were reacted with phosphoric acid at 70°C using a GasBench II connected to a Thermo Finnigan Five Plus mass spectrometer. Carbon and oxygen isotope values are reported in per mil relative to Vienna Pee Dee Belemnite (VPDB) and Vienna Standard Mean Ocean Water (VSMOW), by assigning $\delta^{13}C$ and $\delta^{18}O$ values of +1.95 and –2.20‰ VPDB to NIST reference material NBS19 (limestone), and –46.6 and –26.7‰ VPDB to LSVEC (Li_2CO_3). Reproducibility was checked by replicate analyses of laboratory standards and was ± 0.07‰ (1σ) for both carbon and oxygen isotope analyses.

https://doi.org/10.1180/minmag.2016.080.155 Published online by Cambridge University Press

TABLE 2. Sample label, rock description and associations of the Fiano samples, with minerals listed in order of decreasing abundance.

Sample ID	Rock sample description	Mineral assemblage*
Micaceous xenoliths		
TF1	micaceous xenolith, with red crust	Chn, Phl, Mag, Hem, Grs
TF2	honey-brown micaceous xenolith, with small red crusts	Phl, Fl, Chn, Di, Mag, Rct
TF4	honey-brown micaceous xenolith, with small red crusts	Fl, Phl, Chn, Flb, Di, Mag, Mfr
TF5	micaceous xenolith, with brown and red crusts on a small whitish nucleus	Phl, Fl, Chn, Flb, Di, Cal, Hu, Mag
TF6	micaceous xenolith, with brown and red crusts on a whitish nucleus	Fl, Phl, Flb, Chn, Di, Mag, Cal
TF7	honey-brown micaceous xenolith	Phl, Fl, Mag, Hem, Rct
TF9	micaceous xenolith, with a small white crust	Fl, Phl, Flb, Mag, Hem, Cal
TF10	micaceous xenolith, with red crust	Phl, Fl, Chn, Rct, Hem
TF12	micaceous xenolith, with red crust	Fl, Phl, Chn, Flb, Di, Mag, Mfr
TF13	micaceous xenolith, with red and white crust	Fl, Phl, Chn, Cal, Mag
Carbonate xenoliths		
TF8	poorly metamorphosed carbonate xenolith	Cal
TF11	metamorphosed carbonate xenolith	Cal, Fl, Hem
TF14	poorly metamorphosed carbonate xenolith	Cal
TF15	metamorphosed carbonate xenolith	Cal, Fl, Hem
TF16	poorly metamorphosed carbonate xenolith	Cal

*Cal, calcite; Chn, chondrodite; Di, diopside; Flb, fluoborite; Fl, fluorite; Rct, K-bearing fluoro-richterite; Grs, grossular; Phl, phlogopite; Hem, hematite; Hu, humite; Mag, magnetite; Mfr, magnesioferrite (symbols mainly after Whitney and Evans, 2010).

Six mica single crystals were selected from three micaceous xenoliths for single crystal X-ray diffraction analyses. The same crystals were embedded in epoxy resin and polished to perform electron microprobe (EMP) measurements. A JEOL JXA-8200 electron microprobe (Dipartimento di Scienze della Terra, University of Milan, Italy) operating at 15 kV accelerating voltage, 5 nA sample current on brass, ~1 μm spot size and 40 s counting time. Fluorine, Na, K, Ba, Ca, Cl, Ti, Cr, Mn, Ni, Sr, Zn and Zr contents were analysed by wavelength dispersive spectrometry and Si, Al, Mg and Fe by energy dispersive spectrometry. The used standards were: grossular (Si-Al); forsterite (Mg); omphacite (Na); ilmenite (Ti); rhodonite (Mn); K-feldspar (K); metallic Cr (Cr); fayalite (Fe); wollastonite (Ca); sanbornite (Ba); apatite (F); celestine (Sr); nickeline (Ni); scapolite (Cl); zincian rhodonite (Zn, with ZnO content 7.22 wt.%); and zircon (Zr). Fluorine was analysed following the procedure described in Balassone *et al.* (2013). A *Phi-Rho-Z* routine, as implemented in the JEOL suite of programs, allowed the conversion from X-ray counts to oxide weight percentages (wt.%). Relative uncertainty on the analytical measurements was 1% for major elements and 4% for minor elements. Chromium, Sr, Ni, Zr and Ba were sought for but were found to be below the detection limits (0.04 wt.% for Cr, Ni, Zr; 0.09 wt.% Ba, Zn, Sr; 0.01 wt.% for Ca, Cl).

Single-crystal XRD data were collected by means of a Bruker AXS X8 APEXII automated diffractometer (Dipartimento di Scienze della Terra e Geoambientali, University of Bari Aldo Moro, Italy) equipped with a CCD detector and graphite-monochromatized Mo$K\alpha$ radiation ($\lambda = 0.71073$ Å). The instrument operated at 50 kV, 30 mA and with a 40 mm crystal-to-detector distance. The collection strategy was optimized by the *Apex* program suite by combining several ω and φ rotation scans (scan width 1.0°/frame, exposure time 10 s/frame) and recording the whole Ewald sphere ($\pm h, \pm k, \pm l$) up to $\theta \approx 40°$. The *SAINT* package (Bruker, 2007) was used for the integration of the intensities of reflections and for the correction of Lorentz-polarization. The *SADABS* software (Bruker, 2009) was employed for the absorption correction. Structure refinements were carried out using the *CRYSTALS* software (Betteridge *et al.*, 2003). The

https://doi.org/10.1180/minmag.2016.080.155 Published online by Cambridge University Press

refined parameters were: scale factors, atomic positions, cation occupancies and anisotropic displacement parameters.

Results

Mineral compositions, major- and trace-element geochemistry

The micaceous metamorphosed xenoliths (see Table 2) show locally a geode-like structure and/or zones composed of different mineral assemblages. Their honey-brown parts are rich in idiomorphic mica crystals, which correspond to fluorophlogopite (see the section below for details). Fluorite is widespread and F-rich chondrodite typically forms deep-red crusts. Fluoborite occurs as tiny needles and is fairly common in some xenoliths (Fig. 3*a*,*b*). Other phases detected in small amounts by combined PXRD and EDS analyses are yellow diopside, Fe(Mg)-oxides (magnetite, magnesioferrite and hematite), calcite, humite, K-bearing fluoro-richterite and grossular. Overall they can be classified as calc-silicate rocks (Rosen *et al.*, 2007).

The carbonate metamorphosed xenoliths TF11 and TF15, respectively (Table 2) are mainly composed of calcite with sporadic vuggy fluorite and hematite. They are friable and have saccharoidal texture, hence they can be classified as marbles (Rosen *et al.*, 2007). The three mica-free samples TF8, TF14 and TF16 (Table 2) are compact rocks composed only of calcite and appear to be less affected by thermal metamorphism; accordingly they are here referred to as weakly metamorphosed carbonates.

Selected SEM-BSE images of micaceous xenoliths show that fluorite is ubiquitous, and at least two generations can be observed. It is found in crusts, vugs or fracture fillings (Figs 4*a*–*d*). Sometimes fluorite also occurs as a kind of graphic-like intergrowth in fluoborite (Figs 4*e* and 4*f*). Fluorophlogopite always has a euhedral habit, reaching several millimetres in size. Among other silicates, diopside, chondrodite, grossular and humite generally occur as anhedral crystals and/or aggregates (Fig. 4*g*). Potassium-bearing fluoro-richterite and magnesioferrite are very rare and have not been reported before in the Fiano samples. Other accessory phases are magnetite and hematite (Fig. 4*h*). The mineralogical assemblage in the Fiano xenoliths (Table 2) differs from the mineralogy of Ca-poor ejecta, skarns and marble from the Vesuvius deposits (Barberi and Leoni, 1980; Del Moro *et al.*, 2001; Gilg *et al.*, 2001; Fulignati *et al.*, 2005). Specifically, spinel and brucite do not occur in our samples whereas B-bearing minerals are not reported from the Vesuvian ejecta.

The results of EDS analyses of the Fiano minerals are reported in Table 3. Among silicates, chondrodite and humite are represented by F-rich varieties (as also reported by Balassone *et al.*, 2002). Following Hawthorne *et al.* (2012), the Fiano amphibole can be ascribed to a sodic-calcic variety, and in particular to K-bearing fluoro-richterite, with K = 0.25 atoms per formula unit (apfu). Compared to potassic-fluoro-richterite from Somma-Vesuvius xenoliths (K = 0.67 apfu, Della Ventura *et al.*, 1992), it shows higher F content (~ 2 *vs*. 1.27 apfu in Somma-Vesuvius amphibole). Very low contents of Mg (0.03 apfu) and Mn (0.004 apfu) are found in calcite (Table 3). Fluoborite is close to the end-member $Mg_3(BO_3)F$, with CaO content just above the detection limit (0.03 wt.%) and FeO below the detection limit (Table 3). High amounts of F (24.33 wt.%, Table 3) can be related to the low amount of OH in its composition. Fluorite shows an amount of Mg of 0.12 wt.% ('sellaite' content 0.4%). Hematite shows 2.91 wt.% Al_2O_3 (corundum content 4.3%). Different contents of Al_2O_3 were found in magnesioferrite (4.34 wt.%) and magnetite (0.99 wt.%); magnesioferrite shows an amount of 4.08 wt.% MnO (in terms of end-member composition magnetite 0.50, spinel 7.39, hercynite 0.05, galaxite 0.95, magnesioferrite 80.73, jacobsite 10.38), and magnetite shows 0.73 wt.% MgO, 0.45 MnO wt.% and 0.21 wt.% CaO (magnetite 92.2, spinel 0.10, hercynite 2.11, galaxite 0.04, magnesioferrite 4.11, jacobsite 1.44).

Whole-rock compositions (Table 4) show that Fiano xenoliths are depleted in silica and rich in CaO and MgO, particularly when compared to the Phlegraean magmas (e.g. Piochi *et al.*, 2005; Arienzo *et al.*, 2011; Tomlinson *et al.*, 2012 and references therein). The carbonate xenoliths, e.g. sample TF8, are obviously richest in CaO and most depleted in alkaline elements. The MnO and P_2O_5 concentrations show a large variation (from 0.21 to 0.76 wt.% and from 0.01 to 0.60 wt.%, respectively, see Table 4). Trace-element contents are lower (i.e. *REE*, high-field-strength elements) or comparable (i.e. Cs, Rb, Ba, Th, U, K, Nb, Pb, Sr) to those reported for the Campanian Ignimbrite (Civetta *et al.*, 1997; Polacci *et al.*, 2003; Marianelli *et al.*, 2006; Piochi *et al.*, 2008; Tomlinson *et al.*, 2012). The main difference concerns B and As contents ranging up to several thousand ppm in all samples, except for carbonate xenoliths TF8, TF11 and

https://doi.org/10.1180/minmag.2016.080.155 Published online by Cambridge University Press

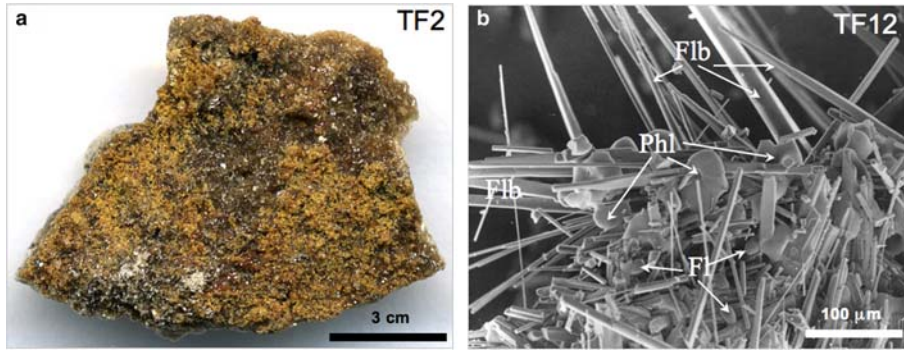

FIG. 3. (*a*) A typical fluorophlogopite-bearing sample from Fiano. (*b*) SEM image of an aggregate of fluoborite (Flb), fluorophlogopite (Phl) and fluorite (Fl).

TF15. The high amount of B (7713 ppm on average) in micacaeous xenoliths is obviously related to fluoborite, whereas As contents (2712 ppm on average) might be due to traces of hörnesite (already found at Fiano), even though this mineral was not detected, at least in the fractions analysed by XRD and EDS, probably due to the intrinsic heterogeneities of the samples. However, the presence of other As-bearing minerals cannot be excluded. As shown in Fig. 5, the *REE* pattern of the Fiano xenoliths is characterized by fractionated light rare-earth elements (*LREE*), negative Eu anomaly, and unfractionated heavy rare-earth elements (*HREE*). Note also that the carbonate xenoliths (yellow symbols in Fig. 5) are slightly depleted in both *LREE* and *HREE* compared to the micaceous ones (red symbols), except for Tm. In addition, the *REE* pattern of the Fiano xenoliths parallels the trend of the Campanian Ignimbrite (blue and green symbols) but are displaced by an order of magnitude to lower *REE* contents. Light *REE* for the Fiano samples overlaps the average of the Somma-Vesuvius marbles and carbonates (peach-coloured band), but the *HREE* are less fractionated, so that Dy and heavier *REE* are present in greater amounts in the Fiano samples than the average for the Somma Vesuvius marbles and carbonates, plausibly a result of the peculiar mineral assemblage. If compared to rocks of Somma-Vesuvius, the xenoliths are richer in selected major and trace elements, such as silica and Cs, Ba, K, Pb, Rb. Also, xenolith TF9 shows the highest Pb content.

Stable isotope geochemistry

The stable isotope data of calcite from both micaceous and carbonate xenoliths are presented in Table 5. The $\delta^{13}C$ and $\delta^{18}O$ values range from –5.2 to 0.0‰ VPDB and 15.7 to 27.1‰ VSMOW, respectively (Table 5). Carbon and oxygen isotopic ratios in the weakly metamorphosed carbonate xenoliths TF14 and TF16 are slightly heavier ($\delta^{13}C$ values of –0.07 and 0.04‰ VPDB; $\delta^{18}O$ values of 26.5 and 24.6‰ VSMOW) compared to the other carbonate xenoliths. Sample TF8, another weakly metamorphosed xenolith, also shows heavier $\delta^{18}O$ value (27.1‰ VSMOW) but a lighter $\delta^{13}C$ (–1.60‰ VPDB) value compared to samples TF14 and TF16. All these values are closer to the isotope values of unmetamorphosed Triassic marine carbonates of the Campanian platform (average $\delta^{18}O$ values = 30‰ VSMOW; average $\delta^{13}C$ = 0.79‰ VPDB; Iannace, 1991) with respect to the other Fiano samples (Fig. 6). The isotope values measured for the Fiano xenoliths overlap those of calcites from thermal metamorphic xenoliths (i.e. marbles and skarns) from Somma-Vesuvius (Gilg *et al.*, 2001). Our values also show a partial correspondence with oxygen and carbon isotope data of the Fiano samples measured by Masi and Turi (1972). However, these authors also report $\delta^{13}C$ values considerably lower than those in this present investigation. As on similar samples from Alban Hills (Turi, 1969), the low to very low $\delta^{13}C$ values (<–15‰) probably result from the complex interaction with meteoric waters (recognized for the external part of nodules plotted in the 'weathering' field of Fig. 6) and from multiple and superimposed decarbonation processes and isotope exchange reactions with hydrothermal fluids, as discussed below. Moreover, the Fiano $\delta^{18}O$ data are much higher than values (8–8.5‰) known for the Campanian Ignimbrite juvenile products (whole rock and feldspar; Taylor *et al.*, 1979) (shaded box in Fig. 6).

https://doi.org/10.1180/minmag.2016.080.155 Published online by Cambridge University Press

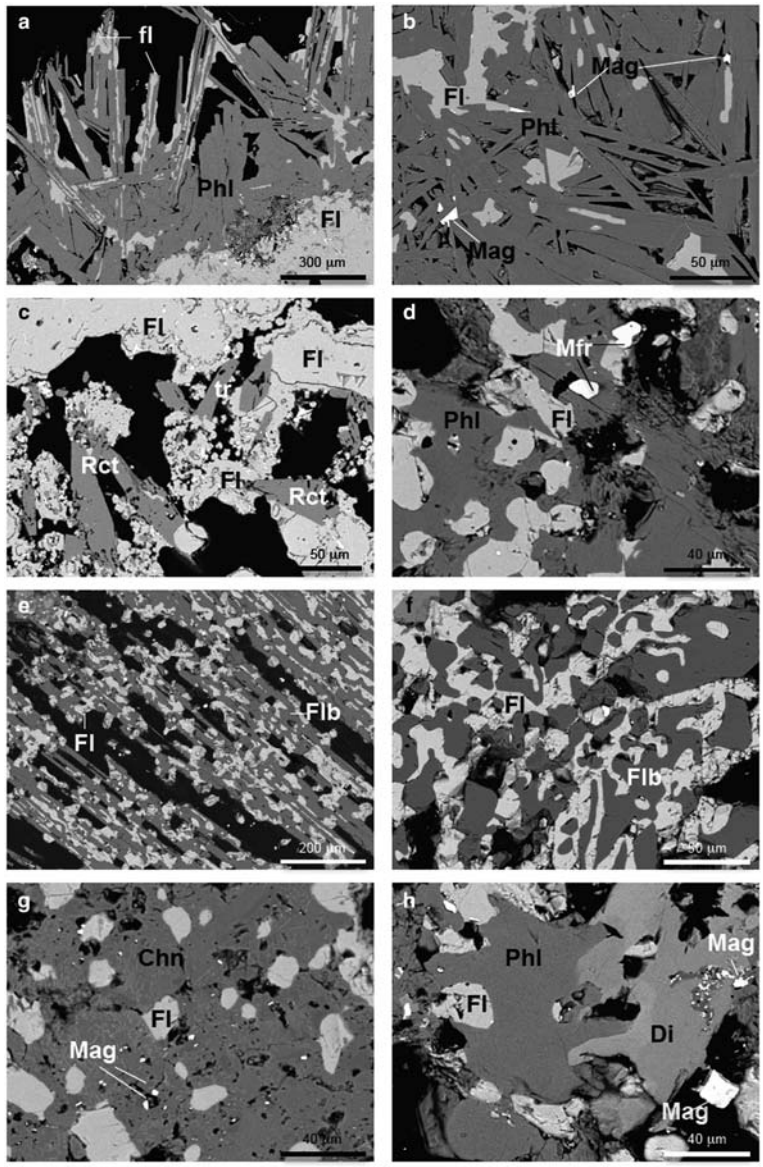

FIG. 4. SEM-BSE micrographs of the mineral assemblage of the Fiano xenoliths. (*a*) fluorophlogopite (Phl) and fluorite (Fl) (sample TF2); (*b*) fluorophlogopite with interstitial fluorite and magnetite (Mag) (sample TF2); (*c*) K-bearing fluoro-richterite (Rct) and fluorite (sample TF2); (*d*) fluorophlogopite, fluorite and magnesioferrite (Mfr) (sample TF4); (*e*) fluoborite (Flb) in needle-like crystals and fluorite (sample TF6); (*f*) enlargement of the previous micrograph; (*g*) chondrodite (Chn) and fluorite, with tiny magnetite crystals (sample TF12); (*h*) diopside (Di), fluorophlogopite and fluorite, with magnetite in both euhedral and tiny anhedral individuals (sample TF12).

Crystal chemistry of fluorophlogopite

Data from EMP indicate close similarities among micas from xenoliths TF2, TF7 and TF10 (Table 6). The crystals studied contain ~43.7 wt.% SiO_2, ~11.1 wt.% Al_2O_3, ~27.2 wt.% MgO, ~2.1 wt.% FeO and ~8.8 wt.% F. These contents are

https://doi.org/10.1180/minmag.2016.080.155 Published online by Cambridge University Press

TABLE 3. Composition (average from six to ten analytical points using EDS, wt.%) and related structural formulae (atoms per formula units) of silicates (*a*) and non-silicates (*b*) found in the Fiano xenoliths.

TABLE 3*a*. Silicates.

Chondrodite		Diopside		K-bearing fluoro-richterite		Grossular		Humite	
SiO_2	33.08	SiO_2	52.85	SiO_2	55.73	SiO_2	39.22	SiO_2	33.04
FeO_t	5.62	FeO_t	6.84	Al_2O_3	0.35	Al_2O_3	22.53	TiO_2	0.29
MgO	54.04	MgO	14.09	FeO_t	1.04	FeO_t	0.45	FeO_t	19.34
MnO	1.05	MnO	0.81	MgO	22.90	MgO	0.13	MgO	41.98
F	10.86	CaO	25.27	MnO	0.26	MnO	0.11	MnO	0.33
Total	104.65	Total	99.86	CaO	10.87	CaO	36.92	CaO	0.09
O = F				K_2O	1.42	Total	99.36	F	5.81
				Na_2O	4.13			Total	100.88
				F	4.57			O = F	–2.44
				Total	101.27			Total	98.44
				O = F	–1.92				
				Total	99.35				
10 (O, OH, F)		6 O		24 (O, OH, F)		24 O		14 (O, OH, F)	
Si	1.95	Si	1.79	Si	7.82	Si	5.94	Si	2.99
Fe	0.28	Fe	0.19	^{IV}Al	0.06	^{IV}Al	0.06	Ti	0.02
Mg	4.75	Mg	0.71	Fe	0.12	^{VI}Al	3.96	Fe	1.46
Mn	0.05	Mn	0.02	Mg	4.79	Fe	0.06	Mg	5.66
F	2.03	Ca	0.92	Mn	0.03	Mg	0.03	Mn	0.03
				Ca	1.63	Mn	0.01	Ca	0.01
				K	0.25	Ca	5.99	F	1.66
				Na	1.12				
				F	2.03				

https://doi.org/10.1180/minmag.2016.080.155 Published online by Cambridge University Press

TABLE 3*b*. Non-silicates.

Calcite		Fluoborite		Fluorite		Hematite		Magnesioferrite[§]		Magnetite[§]	
CaO	54.67	MgO	64.03	Ca	51.00	Fe_2O_3	95.68	Fe_2O_3	74.3	Fe_2O_3	67.57
MgO	0.66	CaO	0.03	Mg	0.12	Al_2O_3	2.91	FeO	0.2	FeO	29.14
MnO	0.14	B_2O_3*	17.30	F	48.00	TiO_2	0.57	Al_2O_3	4.34	Al_2O_3	0.99
FeO	0.49	F	24.33	Total	99.12	Total	99.16	MgO	18.05	MgO	0.73
CO_2*	43.71	H_2O**	2.40					MnO	4.08	MnO	0.45
Total	99.18	Total	108.09					Total	100.97	CaO	0.21
		O = F	−10.24							Total	99.09
		Total 97.85									
2 O		1 B and 3 O		3 O				3 cations		3 cations	
Ca	1.95	Mg	3.07	Ca	1.00	Fe	1.90	Fe^{3+}	1.83	Fe^{3+}	1.96
Mg	0.03	Ca	0.001	Mg	0.004	Al	0.09	Fe^{2+}	0.005	Fe^{2+}	0.94
Mn	0.004	B	1.00	F	1.99	Ti	0.10	Al	0.17	Al	0.04
C	2.00	F	2.47					Mg	0.88	Mg	0.04
		OH	0.53					Mn	0.11	Mn	0.01
										Ca	0.01

*Calculated from stoichiometry; **calculated for a sum (F+OH) = 3 apfu; FeO_t = all Fe as total iron; [§]Fe_2O_3 and FeO calculated according to Droop (1987).

TABLE 4. Whole-rock major element oxides (wt.%) and trace element (ppm) compositions of selected Fiano xenoliths.

Sample ID	TF1	TF2	TF4	TF5	TF6	TF9	TF12	TF8	TF11	TF15
				Micaceous xenoliths					Carbonate xenoliths	
SiO_2	25.33	20.44	13.51	14.00	13.06	14.04	14.76	7.10	5.55	7.33
Al_2O_3	3.59	3.05	2.47	3.06	2.90	4.12	2.75	1.00	1.01	1.50
Fe_2O_3	2.00	1.04	1.19	1.65	1.22	1.00	2.05	0.70	0.52	0.66
MnO	0.32	0.33	0.21	0.24	0.23	0.26	0.70	0.22	0.76	0.25
MgO	29.00	18.54	19.45	22.00	21.13	20.55	18.11	9.88	6.66	9.00
CaO	17.88	30.97	39.11	36.68	39.15	38.95	39.15	41.30	44.53	41.01
Na_2O	1.33	0.55	0.29	0.34	0.30	0.26	0.99	0.07	0.50	0.03
K_2O	2.94	3.00	2.39	2.55	2.05	2.60	2.66	0.60	0.54	0.03
TiO_2	0.11	0.18	0.06	0.09	0.07	0.05	1.70	0.04	0.03	0.01
P_2O_5	0.04	0.30	0.01	0.60	0.01	0.03	0.03	0.01	0.07	0.02
LOI	16.73	20.66	20.65	17.11	19.00	17.00	16.90	38.99	40.00	39.43
Total	99.27	99.06	99.34	98.32	99.12	98.86	99.80	99.95	100.17	99.27
Be	4.2	5.0	8.0	7.7	8.1	6.7	4.9	2.0	3.0	3.0
B	8991	4567	7421	8965	8065	8991	6993	100	98	102
Sc	2	1	–	1.0	–	–	1.0	–	–	–
V	53	44	49	47	51	52	48	30	57	33
Cr	23	27	20	22	23	24	24	12	19	13
Co	4	3.3	2.8	2.9	3	2.3	4	0.5	3	0.5
Ni	0.9	0.6	0.5	0.6	0.49	0.61	0.52	11	9	12
Cu	7.6	8	8.1	7.65	7.9	7.1	6.95	8	7	9
Zn	373.1	334	304	299	293	279	307	156	163	154
Ga	5	5.2	4.4	4	5	5	4.8	4	5.5	3
As	2788	2800	2502.2	3007	2574	2812	2500	12	150	16
Se	2	1.1	1	2	1.3	1.5	2	0.5	2	0.4
Rb	431	447	401.6	500	408	399	411	59	104	50
Sr	112	132	103.4	96	100	100	99	399	170	200
Y	4.2	4	3.9	5	4.4	4	4.7	1	7	2
Zr	29	31	34.4	25	28	27	29	8	17	9
Nb	15.3	14	14.1	14	15	14.1	14.5	4	9	5
Mo	2.4	2	1.5	3	2	3.2	2	6	5	5
Ag	0.7	0.7	0.5	1	1	1.1	1.2	0.4	1	0.45
Cd	0.12	0.09	0.05	0.06	0.10	0.1	0.11	0.2	0.1	0.22
Sn	32	26	29	33	30	30	33	2.3	19	2.4

Sb	6	6.3	7.2	7	6	8	7	1	5	2
Cs	57	59	65.7	59	58	60	62	3	20	4
Ba	18	18.1	17	16	16.8	16.4	17	26	20	28
La	5.7	5.99	6	5.73	6.11	5.44	5.7	3.7	4.5	3.9
Ce	10.7	10.6	10.8	10.6	10.5	10	10.54	7.85	8.9	8
Pr	1.1	1.21	1.22	1.1	1.16	1.03	1.04	0.71	0.96	0.8
Nd	4	4.2	4.4	4	3.9	3.8	3.91	2.1	2.9	2.5
Sm	0.6	0.62	0.62	0.6	0.63	0.59	0.56	0.4	0.45	0.41
Eu	0.1	0.1	0.08	0.09	0.08	0.09	0.082	0.06	0.069	0.057
Gd	0.51	0.5	0.57	0.44	0.52	0.49	0.52	0.39	0.43	0.35
Tb	0.08	0.079	0.09	0.082	0.087	0.085	0.087	0.06	0.063	0.055
Dy	0.45	0.46	0.56	0.49	0.5	0.5	0.53	0.33	0.36	0.358
Ho	0.09	0.092	0.11	0.096	0.099	0.095	0.1	0.07	0.077	0.071
Er	0.25	0.27	0.33	0.29	0.285	0.3	0.3	0.19	0.22	0.2
Tm	0.033	0.037	0.04	0.038	0.039	0.04	0.039	0.027	0.03	0.029
Yb	0.24	0.26	0.32	0.289	0.299	0.3	0.25	0.17	0.2	0.186
Lu	0.037	0.039	0.05	0.044	0.045	0.046	0.038	0.027	0.031	0.029
Hf	0.8	0.66	0.6	0.7	0.71	0.65	0.73	0.02	0.68	0.03
Ta	0.9	0.76	0.6	0.72	0.66	0.7	0.68	0.05	0.36	0.05
W	8	7.99	8.9	9	8.5	9.1	8.8	0.6	8	0.7
Au*	15	14	14.4	13.9	14.3	13.6	14	5	8	6.1
Hg	0.6	0.5	0.33	0.32	0.35	0.33	0.33	0.2	0.3	0.3
Tl	0.2	0.2	0.3	0.2	0.22	0.22	0.19	0.1	0.2	0.11
Pb	76	79	77.9	81	79	80	75	200	76	203
Bi	0.7	0.5	0.5	0.7	0.6	0.65	0.6	2.9	0.55	2.6
Th	1.3	1.37	1.4	1.45	1.45	1.7	1.3	0.7	1.6	0.8
U	6	5.7	5.5	5	6	5.3	5.1	0.8	2.5	0.9

– not detected. *ppb.

https://doi.org/10.1180/minmag.2016.080.155 Published online by Cambridge University Press

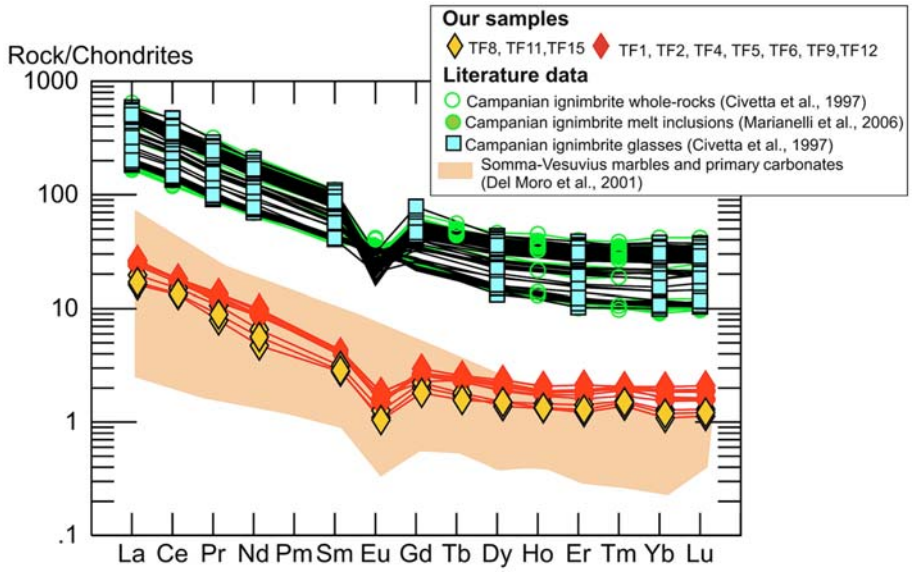

FIG. 5. *REE* distribution pattern for the studied xenoliths (red and yellow diamonds for the micaceous and carbonate xenoliths, respectively) in the field of Somma-Vesuvius marble and unmetamorphosed limestone (Del Moro *et al.*, 2001) compared with data from whole-rock (unfilled circle: data from Civetta *et al.*, 1997), melt inclusions (filled circles: data from Marianelli *et al.*, 2006) and glassy matrix (filled squares: data from Civetta *et al.*, 1997) of the Campanian Ignimbrite. Values normalized on the basis of McDonough and Sun (1995).

essentially the same as that found in the Vesuvius fluorophlogopite from the 1872 eruptions (Balassone *et al.*, 2013), i.e. those of near end-member F species with high Mg and negligible Al in the octahedral sites. Caesium is detected in whole-rock analysis (up to 65.7 ppm, see Table 4) but was not searched for in micas. However, even if it were completely partitioned into the mica, its content would be <0.001 apfu, negligible from a crystal chemical viewpoint.

The results of the structure refinements (see the values of the R_1, wR_2, $\Delta\rho_{min}/\Delta\rho_{max}$ and Goof in Table 7), carried out in the expected *C2/m* space group for polytype 1*M* indicate good data and crystal quality. Lattice parameters (on average $a \approx 5.30$, $b \approx 9.19$, $c \approx 10.13$ Å, $\beta \approx 100.08°$, Table 7), structure data (supplementary Table S1 – all supplementary tables have been deposited with the Principal Editor of *Mineralogical Magazine* and are available from http://www.minersoc.org/pages/e_journals/dep_mat_mm.html), mean bond-length distances (<T–O> ≈ 1.65, <M–O> ≈ 2.06, <K–O> ≈ 3.13 Å, supplementary Table S2) and polyhedral distortional parameters (supplementary Table S3) are very similar for all the analysed crystals, confirming the substantial compositional and structural homogeneity, already established on the basis of EMP data. The crystals investigated are geometrically 'homo-octahedral' (i.e. <M1–O> equals the <M2–O> distances within three standard deviations, Weiss *et al.*, 1992). This geometrical feature is consistent with a disordered cation distribution at octahedral sites. A comparison between the mean atomic numbers of cation sites as determined by structure refinement and those calculated from the chemical molar fractions and atomic radii in Shannon (1976) is reported in the supplementary Table S4. The combination of EMP and SCXRD data leads to the structural formulae given in Table 8. They were calculated following the procedure described in Ottolini *et al.* (2012) and Schingaro *et al.* (2013). Note that the formulae of the samples studied are similar to those of the Vesuvius fluorophlogopite from the 1872 eruptions (Balassone *et al.*, 2013), apart from a small tetraferriphlogopite component and a greater variability in $^{VI}Fe^{3+}$ content. These data show that the Fiano micas are fluorophlogopite with minor tetraferriphlogopite component. Al,Fe^{3+}-vacancy [$3\,^{VI}M^{2+} \leftrightarrow 2\,^{VI}M^{3+} + {}^{VI}\square$] and $^{XII}K^{+} + {}^{IV}Al^{3+} \leftrightarrow {}^{IV}Si^{4+} + {}^{XII}\square$ substitutions also occur. The structural effects of $OH^{-} \rightarrow F^{-}$ substitution in

https://doi.org/10.1180/minmag.2016.080.155 Published online by Cambridge University Press

TABLE 5. Oxygen and carbon isotope compositions of calcite from selected Fiano xenoliths.

Sample	$\delta^{13}C$ (‰ VPDB)	$\delta^{18}O$ (‰ VPDB)	$\delta^{18}O$ (‰ VSMOW)
Micaceous xenoliths			
TF5	–4.28	–14.72	15.68
TF6	–5.20	–9.43	21.13
TF9	–1.61	–11.15	19.37
TF13	–0.64	–7.13	23.51
Carbonate xenoliths			
TF8	–1.60	–3.62	27.12
TF11	–4.31	–10.47	20.06
TF14	–0.07	–4.28	26.45
TF15	–3.89	–11.01	19.51
TF16	0.04	–6.12	24.56

micas were reviewed recently by Balassone *et al.* (2013). Fluorophlogopite is interesting in showing structural distortions mainly along the direction close to the K–O4 bond with a consequent shrinkage of *c*-cell parameter, K–O4 distance, Δ_{K-O} (i.e. difference between $<K–O>_{outer}$ and $<K–O>_{inner}$

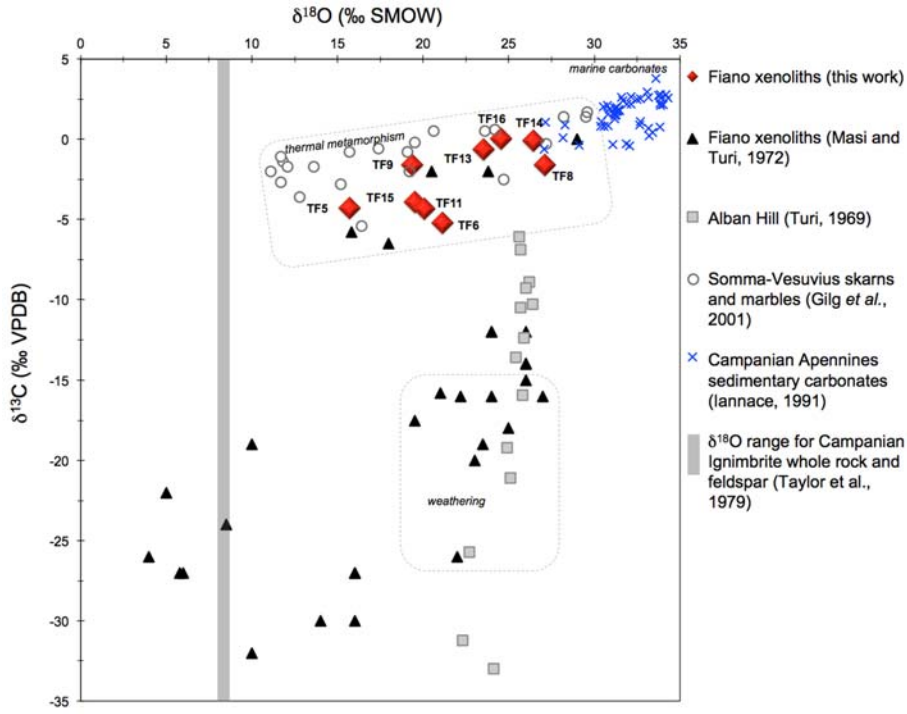

FIG. 6. Plot of carbon *vs*. oxygen isotope values of the Fiano xenoliths and comparison with literature data. The 'thermal metamorphism' field depicts the range of isotopic compositions of calcites from metalimestones, metadolostones and skarns of Somma-Vesuvius after Gilg *et al.* (2001), and some of the metamophosed Fiano xenoliths after Masi and Turi (1972); the 'weathering' field represents the isotopic composition of outer shells of the Fiano xenoliths affected by exchange process with meteoric water (Masi and Turi, 1972). The range of $\delta^{18}O$ for Campanian Ignimbrite whole rocks and feldspar from Taylor *et al.* (1979) is also reported. See text for further discussion.

https://doi.org/10.1180/minmag.2016.080.155 Published online by Cambridge University Press

TABLE 6. Representative compositions (wt.%) and atomic ratios (apfu) calculated on the basis of 12(O, OH, F) of Fiano micas.

Sample	TF2_1	TF2_2	TF7_1	TF7_2	TF10_1	TF10_2
SiO_2	43.6(2)	44.0(2)	43.7(3)	43.7(3)	44.2(2)	43.2(2)
Al_2O_3	11.0(1)	12(1)	10.8(5)	10.8(2)	11.1(5)	10.8(6)
MgO	26.3(3)	25.9(2)	28.1(7)	28.0(2)	27.9(4)	27.2(2)
FeO_t^a	3.1(1)	2.9(2)	2.0(3)	1.5(2)	1.5(2)	1.6(1)
TiO_2	0.10(3)	0.08(2)	0.06(3)	0.09(3)	0.13(5)	0.09(3)
MnO	0.26(4)	0.21(4)	0.14(3)	0.19(4)	0.25(6)	0.33(1)
ZnO	b.d.l.	b.d.l.	b.d.l.	0.13(9)	b.d.l.	b.d.l.
K_2O	9.38(7)	9.17(8)	9.62(8)	9.67(4)	9.69(4)	9.12(6)
Na_2O	0.76(2)	0.91(1)	0.57(4)	0.65(4)	0.57(4)	0.79(2)
CaO	b.d.l.	b.d.l.	0.06(6)	0.10(6)	b.d.l.	b.d.l.
F	8.0(2)	8.9(1)	9.1(2)	9.1(1)	8.9(1)	8.9(5)
Cl	b.d.l.	0.08(3)	b.d.l.	b.d.l.	b.d.l.	b.d.l.
Total	102.5(3)	104(1)	104.2(7)	103.9(2)	104.2(8)	102(1)
O = F, Cl	–3.39	–3.78	–3.82	–3.84	–3.76	–3.75
	99.11	100.22	100.38	100.06	100.44	98.25
Si	3.06	3.06	3.05	3.05	3.06	3.06
^{IV}Al	0.85	0.93	0.88	0.87	0.91	0.91
^{IV}Fe	0.09	0.00	0.06	0.08	0.03	0.03
sum	4.00	3.99	3.99	4.00	4.00	4.00
^{VI}Al	0.05	0.03	0.00	0.02	0.00	0.00
Mg	2.75	2.69	2.91	2.92	2.89	2.88
$^{VI}Fe_t$	0.09	0.17	0.05	0.01	0.05	0.06
Ti	0.01	0.00	0.00	0.00	0.01	0.00
Mn	0.02	0.01	0.01	0.01	0.01	0.02
Zn	0.00	0.00	0.00	0.01	0.00	0.00
sum	2.92	2.92	2.97	2.97	2.96	2.96
K	0.84	0.81	0.86	0.86	0.86	0.82
Na	0.10	0.12	0.08	0.09	0.08	0.11
Ca	0.00	0.00	0.00	0.01	0.00	0.00
sum	0.94	0.94	0.94	0.96	0.94	0.93

[a]FeO_t is total iron; bdl = below detection limit.

distances) and interlayer thickness (t_{int} parameter). The values of these parameters for samples TF2, TF7 and TF10 match very well to those determined for other fluorophlogopite samples (e.g. compare Supplemental Data Table S3 of this work with Supplemental Data table 3 in Balassone *et al.*, 2013). Incorporation of fluorine is also accompanied by reduction of the ditrigonalization of the T sheet and, therefore, by decrease of the in-plane rotation angle (α). This also holds for the Fiano micas that exhibit α values in the range 6–6.40°. Consequently, the micas plot very close to end-member fluorophlogopite (Fig. 7) whereas, according to Schingaro *et al.* (2011), very low values of the α correspond to micas affected by extensive $OH^- \rightarrow F^-$ and by significant de-hydrogenation.

Discussion

Mineral association and genetic conditions

The natural variability of fluorine concentration in mica, ideally from 0–2 F apfu, is broadly reflected in the variation of the α distortional parameter from 4–11°. In Fig. 7 small amounts of F correspond to a very large difference in α. This parameter, as well as all the other crystal chemical features of the mica studied from the TF2, TF7 and TF10 xenoliths,

https://doi.org/10.1180/minmag.2016.080.155 Published online by Cambridge University Press

TABLE 7. Crystallographic data for the micas studied.

	TF2_1	TF2_2	TF7_1	TF7_2	TF10_1	TF10_2
Crystal size (mm)	0.35x0.15x0.01	0.38x0.19x0.03	0.45x0.25x0.02	0.46x0.39x0.06	0.48x0.47x0.04	0.65x0.47x0.02
Space group	*C2/m*	*C2/m*	*C2/m*	*C2/m*	*C2/m*	*C2/m*
a (Å)	5.3030(1)	5.3002(1)	5.3044(3)	5.3056(1)	5.3047(1)	5.3083(1)
b (Å)	9.1866(2)	9.1830(2)	9.1891(4)	9.1925(2)	9.1882(2)	9.1919(3)
c (Å)	10.1298(2)	10.1298(2)	10.1360(6)	10.1288(3)	10.1298(2)	10.1291(3)
β (°)	100.074(2)	100.046(1)	100.109(4)	100.077(2)	100.071(1)	100.093(2)
Cell volume (Å^3)	485.88(2)	485.48(2)	486.39(5)	486.38(2)	486.13(2)	486.58(2)
Z	4	4	4	4	4	4
Reflections collected	4955	4985	3876	6027	6405	5980
Reflections unique	1239	1241	1241	1768	1745	1785
$R_{merging}$ [$R_{(int)}$] (%)	3.13	2.23	4.11	1.65	1.85	2.16
Reflections used ($I > 3\sigma(I)$)	950	1041	834	1495	1430	1330
No. of refined parameters	63	63	61	61	61	61
Goof[a]	1.110	1.051	1.062	1.045	1.041	1.101
R_1[b] (%)	2.68	1.99	4.37	1.78	1.92	2.48
wR_2[c] (%)	2.50	2.82	5.10	2.21	2.28	2.71
$\Delta\rho_{min}/\Delta\rho_{max}$ (e^-/Å^3)	–0.41/0.53	–0.23/0.61	–0.81/0.57	–0.21/0.41	–0.33/0.43	–0.37/0.65

a: Goodness-of-fit = $[\Sigma[w(F_o^2–F_c^2)^2]/(N–p)]^{1/2}$, where N and p are the number of reflections and parameters, respectively.

b: $R_1 = \Sigma[|F_o| - |F_c|]/\Sigma|F_o|$.

c: $wR_2 = [\Sigma[w(F_o–F_c)^2]/\Sigma[w(F_o)^2]]^{1/2}$; w = Chebyshev optimized weights.

TABLE 8. Structural formulas in atoms per formula unit (apfu) for the micas studied.

	Interlayer	Octahedral site	Tetrahedral site	Anionic site
TF2_1	$(K_{0.84}Na_{0.10})_{\Sigma=0.94}$	$(Mg_{2.75}Mn_{0.02}Fe^{3+}_{0.09}Al_{0.05}Ti_{0.01}\square_{0.08})_{\Sigma=3.00}$	$(Si_{3.06}Al_{0.85}Fe^{3+}_{0.09})_{\Sigma=4.00}$	$O_{10.01}OH_{0.21}F_{1.78}$
TF2_2	$(K_{0.81}Na_{0.12})_{\Sigma=0.93}$	$(Mg_{2.69}Mn_{0.01}Fe^{3+}_{0.17}Al_{0.02}\square_{0.11})_{\Sigma=3.00}$	$(Si_{3.06}Al_{0.94})_{\Sigma=4.00}$	$O_{10.00}OH_{0.03Cl0.01}F_{1.96}$
TF7_1	$(K_{0.86}Na_{0.08})_{\Sigma=0.94}$	$(Mg_{2.91}Mn_{0.01}Fe^{3+}_{0.04}\square_{0.04})_{\Sigma=3.00}$	$(Si_{3.05}Al_{0.88}Fe^{3+}_{0.07})_{\Sigma=4.00}$	$O_{10.00}F_{2.00}$
TF7_2	$(K_{0.86}Na_{0.08}Ca_{0.01})_{\Sigma=0.96}$	$(Mg_{2.92}Mn_{0.01}Zn_{0.01}Fe^{3+}_{0.01}Al_{0.02}\square_{0.02})_{\Sigma=2.98}$	$(Si_{3.05}Al_{0.87}Fe^{3+}_{0.08})_{\Sigma=4.00}$	$O_{10.00}F_{2.01}$
TF10_1	$(K_{0.86}Na_{0.08})_{\Sigma=0.93}$	$(Mg_{2.89}Mn_{0.01}Fe^{3+}_{0.05}Ti_{0.01}\square_{0.04})_{\Sigma=3.00}$	$(Si_{3.06}Al_{0.91}Fe^{3+}_{0.03})_{\Sigma=4.00}$	$O_{10.00}OH_{0.04}F_{1.96}$
TF10_2	$(K_{0.82}Na_{0.11})_{\Sigma=0.93}$	$(Mg_{2.88}Mn_{0.02}Fe^{3+}_{0.06}\square_{0.03})_{\Sigma=2.99}$	$(Si_{3.06}Al_{0.91}Fe^{3+}_{0.03})_{\Sigma=4.00}$	$O_{10.00}F_{2.00}$

closely approach those of the end-member fluorophlogopite in Gianfagna *et al.* (2007) and Balassone *et al.* (2013), regardless of their different parageneses. Specifically, fluorophlogopite in benmoreitic lava at Biancavilla (Catania, Mount Etna, Sicily) is associated with fluoro-edenite, alkali-feldspars, clino- and ortho-pyroxenes, fluorapatite, hematite and pseudobrookite. The genesis of this mineral assemblage was ascribed to F- and Cl-rich fluids that have locally metasomatized the benmoreite (Gianfagna *et al.*, 2007). Fluorophlogopite in xenoliths from the Vesuvius AD 1872 eruption (Balassone *et al.*, 2013), instead, was found in association with anhydrous osumilite, sodalite and gypsum. It was hypothesized that the xenoliths formed in a high-temperature (>700°C) low pressure (<1 kbar) environment from a magma-body-sourced volatile component characterized by a high concentration of F and a minor concentration of Cl and S.

Although fluorophlogopite is found in diverse mineral assemblages (Gianfagna *et al.*, 2007; Balassone *et al.*, 2013; Scordari *et al.*, 2013; Schingaro *et al.*, 2014), it invariably indicates the presence of a significant volatile content in the system. In the present study, fluorophlogopite from the micaceous xenoliths is associated mainly with fluorite, F-rich chondrodite and fluoborite, and subordinately to diopside, magnetite, magnesioferrite, hematite, calcite, humite, K-bearing fluororichterite and grossular, which define a rare and peculiar F (Mg)-rich mineral assemblage. It can be observed that: (1) fluoborite is a relatively rare borate mineral only described in magnesian skarns worldwide (see Marincea, 2000 and review therein) in association with chondrodite, norbergite and fluorite; (2) humite-group minerals occur in some metamorphosed silica-deficient dolostones and limestones (Mg hornfelses and skarns) together with other species, such as diopside, tremolite and spinel (Tell, 1974); and (3) K-bearing fluororichterite rarely occurs in metamorphic environments; exceptions are, for instance, the thermometamorphic ejecta from Somma-Vesuvius volcano, Italy (Della Ventura *et al.*, 1992), and the amphibole-diopside metacherts in marble from Bufa del Diente, Mexico (Heinrich, 1994).

According to Marincea (2000), crystallization of fluorophlogopite and fluoborite requires a substantial activity of fluorine in the boron-bearing metasomatic fluids. Experimentally, 'fluoborite' is stable at a temperature of 380–450°C (Tell, 1974). This is consistent with data on humite that crystallizes from fluorine reactions in silica-deficient

https://doi.org/10.1180/minmag.2016.080.155 Published online by Cambridge University Press

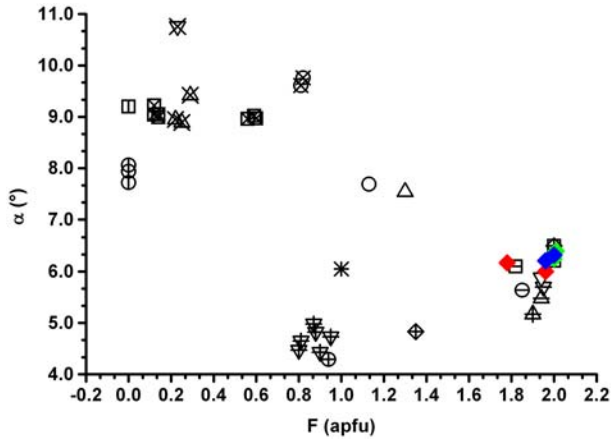

FIG. 7. Plot of ditrigonalization parameter (α) *vs.* F content for micas affected by variable extent of $OH^- \rightarrow F^-$ substitution. Symbols: Solid diamonds indicate the phlogopites in this study: red for the TF2; green for the TF7; blue for the TF10 crystals. Open symbols for literature fluorophlogopites (square: Takeda and Donnay, 1966; circle: Joswig, 1972; triangle pointing upward: Hazen and Burnham, 1973; triangle pointing downward: McCauley *et al.*, 1973; diamond: Takeda and Morosin, 1975; square with plus inside: Hazen *et al.*, 1981; circle with plus inside: Russell and Guggenheim, 1999; triangle pointing upward with plus inside: Gianfagna *et al.*, 2007; triangle pointing downward with plus inside: Schingaro *et al.*, 2011; diamond with plus inside: Scordari *et al.*, 2013; star: Schingaro *et al.*, 2014; square, circle, triangle pointing upward and triangle pointing downward with horizontal line: Balassone *et al.*, 2013). Open symbols with vertical bar inside for literature de-hydrogenated phlogopites and end member phlogopite (square: Redhammer and Roth, 2002; circle: Cesare *et al.*, 2003). Open symbols with cross inside are phlogopites from Balassone *et al.* (2013).

dolomite between 300 and 560°C, in the pressure range from 700–2000 bar (Tell, 1974). This is also in agreement with the temperatures <500–600°C at a pressure of <1kbar which are involved in the occurrence of the K-bearing fluoro-richterite in the metamorphic rocks. Specifically, these conditions were suggested by the breakdown of dolomite *via* the reaction dolomite + SiO_2 = diopside + CO_2 (Della Ventura *et al.*, 1992) in the case of the Somma Vesuvius ejecta.

The potassic-fluoro-richterites from metacherts of Mexico were considered to be formed by the reaction of early diopside formed by contact-metamorphism with pervasive hypersaline brines of magmatic origin (Heinrich, 1994). The Fiano K-bearing fluoro-richterite have similarly formed in the presence of similar F-Na-K(Ca)-rich and Cl-free metasomatic brines at similar temperatures (c. 500°C), even if at lower *P* conditions. We have observed diopside grains enclosed in K-bearing fluoro-richterite; this evidence might also lead to infer amphibole formation at the expense of clinopyroxene, implying infiltration of metasomatic brines after peak metamorphism (Heinrich, 1994).

The halogen content of fluorophlogopite can be used to evaluate the relative fugacities of H_2O and HF in the fluids using the procedure in Cesare *et al.* (2003). For this calculation the value of the exchange temperature is required. The peak value of biotite crystallization should not be used because the halogen and hydrogen contents of mica may not be primary (Cesare *et al.* 2003), as also discussed above. However, considering our mineral assemblage and the discussion above we calculated the log (fH_2O)/(fHF), (fH_2O)/(fHCl) and (fHF)/(fHCl) both at 300° and 500°C. The obtained values were 4.1, 4.9 and –1.3 at 300°C and 3.1, 3.7 and –0.9 at 500°C, in both cases indicating that the role of water overwhelms that of other volatiles. Trace-element and stable isotope geochemistry support the previous considerations and provide additional geochemical clues pointing to metasomatism for the Fiano xenoliths.

In particular, the *REE* patterns of the Fiano samples are similar to Somma-Vesuvius metamorphosed and unmetamorphosed carbonate ejecta. However, the enrichment of B, As, Se and Hg in the Fiano xenoliths (Table 4) compared to the carbonates and marbles of Somma-Vesuvius is consistent

https://doi.org/10.1180/minmag.2016.080.155 Published online by Cambridge University Press

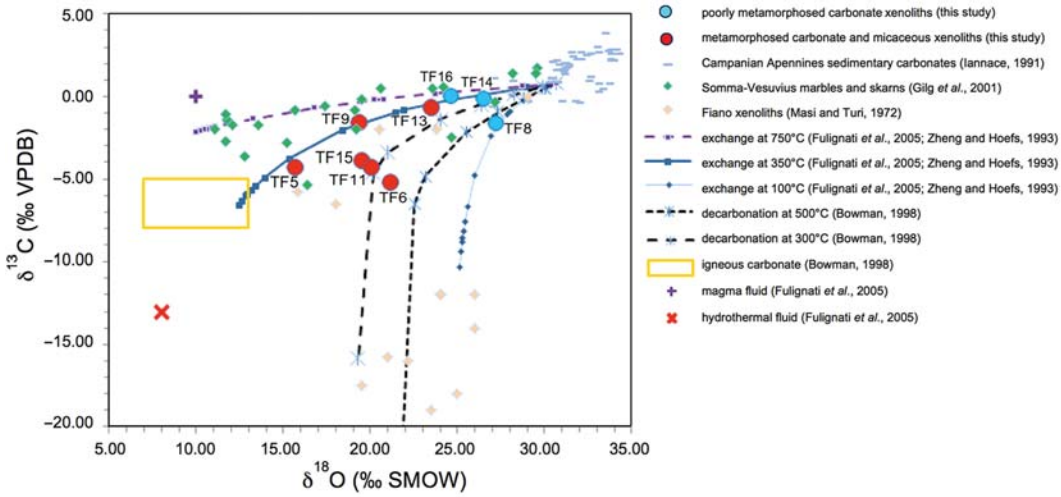

FIG. 8. Covariation of C and O isotope composition as from modelling of interaction between an initial sedimentary carbonate (limestone with $\delta^{13}C = 0.79‰$ VPDB and $\delta^{18}O = 30‰$ VSMOW, average from Iannace, 1991) and a hydrothermal fluid with $\delta^{13}C = –13‰$ VPDB and $\delta^{18}O = 8‰$ VSMOW in the temperature range 100–350°C (as derived by mineralogical data), or a magmatic fluid with $\delta^{13}C = 0‰$ VPDB and $\delta^{18}O = 10‰$ VSMOW at 750°C (following Fulignati *et al.*, 2005). Modelling made following Zheng and Hoefs (1993). Points along the lines are the fluid/rock ratio from 0 at the not modified limestone value to 1 at the opposite side as maximum exchange. The plot also shows the decarbonation modelling through Rayleigh processes (Bowman, 1998). In such a case, points along the lines indicate element (O, C) fractionation from any, e.g. 0.01, to maximum possible, e.g. 1, isotope fractionation. For the calculation we used equilibrium isotopic fractioning values $\alpha = (1000 + \delta^{13}C)$calcite/$(1000 + \delta^{13}C)$fluid and $(1000 + \delta^{18}O)$calcite/$(1000 + \delta^{18}O)$fluid, fluid properly recalculated as a function of temperature after Bottinga (1968), in the various systems: $CaCO_3$–H_2O and $CaCO_3$–HCO_3 for the exchanges at 100° and 350°C, $CaCO_3$–H_2O and $CaCO_3$–CO_2, for the exchanges at 750°C, and $CaCO_3$–CO_2 for decarbonation.

with the easy mobilization of B during prograde metamorphism (Leeman *et al.*, 1992). This is also supported by the observation that the samples with lower $\delta^{18}O$ values (e.g. TF5 and TF9 in Fig. 6), i.e. far from the sedimentary protolith, are rich in B and As (Table 4).

In addition, the carbon and oxygen isotopes of the Fiano xenoliths indicate a depletion trend of ^{13}C and ^{18}O as observed similarly in the Somma-Vesuvius nodules (see Fig. 6), with the lower values being related to metamorphism at a host-rock magma interface (Gilg *et al.*, 2001). Multistage fractionation processes, which were evident in the very light carbon isotope ratios reported for the Fiano carbonate xenoliths by Masi and Turi (1972), are not apparent in this study.

The covariation in C and O isotopes are shown in Fig. 8 as well as the expected equilibrium values based on calcite-fluid interaction (Zheng, 1990; Zheng and Hoefs, 1993) and decarbonation processes (Bowman, 1998) at different temperatures, based on mineralogy. The distribution of the isotope values can be related to the interaction of a hydrothermal fluid dominated by HCO_3^- with the carbonate deposits at 100–350°C. This is consistent with high values of the relative fugacity of H_2O calculated from the fluorophlogopite composition of the xenoliths (see above). The end-member used for hydrothermal fluids has typically an isotope composition of $\delta^{13}C = –13‰$ VPDB and $\delta^{18}O = 8‰$ VSMOW (Zheng and Hoefs, 1993). In addition, a temperature of ~300°C required for the isotopic shift is in agreement with the stability conditions of the newly-formed fluorophlogopite. However, the isotope ratios cannot be explained by the interaction of a magmatic fluid ($\delta^{13}C = 0‰$ VPDB and $\delta^{18}O = 10‰$ VSMOW) with the Mesozoic sedimentary carbonate (see 'exchange at 750°C' in Fig. 8), as modelled by Fulignati *et al.* (2005). Moreover, decarbonation at 300°C or 500°C cannot explain the observed variation in $\delta^{13}C$ of up to about >–5‰, although this process is in agreement with the lighter isotope values of the Fiano carbonates that were reported by Masi and

https://doi.org/10.1180/minmag.2016.080.155 Published online by Cambridge University Press

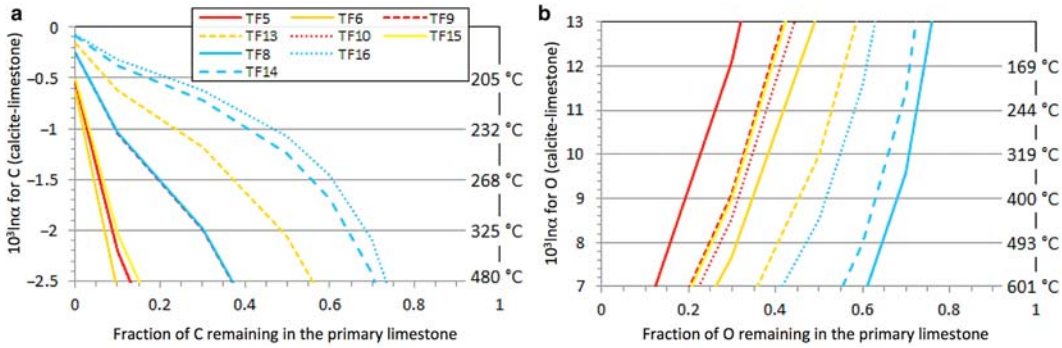

FIG. 9. Calculated $10^3\ln\alpha$ *vs*. oxygen (*a*) and carbon (*b*) fractionation recalculated considering decarbonation of the initial carbonate (average from Iannace, 1991) and determined values of $\delta^{18}O$ and $\delta^{13}C$. Modelling is carried out using the formula of Zheng and Hoefs (1993) and Bowman (1998), whereas the temperatures on the right side of the diagrams are derived from Bottinga (1968) based on equilibrium isotopic fractioning values α as in Fig. 8.

Turi (1972). Assuming a Rayleigh decarbonation process (Fig. 9), we plotted the carbon and oxygen isotope fractionation between calcite and fluid, $10^3\ln\alpha$, where $\alpha = (1000 + \delta^{13}C)_{calcite}/(1000 + \delta^{13}C)_{fluid}$ or $(1000 + \delta^{18}O)_{calcite}/(1000 + \delta^{18}O)_{fluid}$, on the basis of the measured isotope values (final calcites) relative to the fraction, *F*, of carbon or oxygen left in primary calcite (Mesozoic carbonate). Only the reasonable ranges (Bottinga, 1968) of calculated $10^3\ln\alpha$ values are displayed in Fig. 9. Considering both modelling and the upper oxygen limit for carbonate ($F > 0.6$; Bowman, 1998), we suggest that decarbonation at ~450°, as derived (see above) by stability temperature for fluoroborite and phlogopite, probably affected the weakly metasomatized Fiano xenoliths (TF8, TF14 and TF16 samples). Moreover, following Bowman (1998), the calculated $10^3\ln\alpha$ and *F* values indicate conditions intermediate between 'silicatic' disequilibrium and 'silica-absent' decarbonation. Therefore, the scatter in Fig. 8 can also be derived partially from an initial decarbonation process prior to the main hydrothermal alteration of the primary carbonates, within the pyroclastic flow.

Volcanological implications

The Campanian Ignimbrite pyroclastic flow emplaced at Fiano had a temperature range of 300–500°C and underwent hydrothermal processes during its cooling, as registered from the mineralogy and isotope composition of the embedded xenoliths. The intense lithification of the ignimbrite (Cappelletti *et al.*, 2003) and the remnant magnetic susceptibility (e.g. Ort *et al.*, 1999) indicate temperatures of ~400°C during the Campanian Ignimbrite emplacement and are consistent with our estimates. Apparently, the fluorine- and boron-rich fluids circulated during and/or after the ignimbrite emplacement. Indeed, the xenoliths occur in the uppermost portion of the thick ignimbrite sequence and were not subjected to the density and size effects expected in pyroclastic flow currents. The secondary crystallization, as well as the contraction phenomena of some xenoliths described in the literature (Masi and Turi, 1972; Carati, 1987), was the consequence of metasomatic fluids acting on the carbonate xenoliths within the emplacing ignimbrite. This non-quantifiable phenomenon was probably the cause of the expected oxygen and carbon loss during the metasomatic process, as described in the literature (Bowman, 1998).

On the basis of the fluorophlogopite crystal chemistry and the isotope modelling, we suggest that hydrothermal fluids circulating in the pyroclastic flow were dominated by H_2O-rich fluids with only minor chlorine and fluorine. As the zeolite formation and the geochemistry of the micaceous xenoliths testify, these hot fluids were saline and probably provided F and B, as well as As and K, that were absent in both marbles and primary limestones (Table 4). Primary biotites of the Campanian Ignimbrite have fluorine contents that are much lower (0.7 to 2.5 wt.%, see the 'Volcanological context' section above) than phlogopite of the Fiano xenoliths (up to 9.1 wt.%; Tables 3 and 6). Moreover, the glassy matrix was not able to trap fluorine, as their F contents overlap with

https://doi.org/10.1180/minmag.2016.080.155 Published online by Cambridge University Press

those of the melt inclusions (0.26 to 0.89 wt.%, see the 'Volcanological context' section). Similarly, the Campanian Ignimbrite rocks have B contents less than a few tens of ppm (Tonarini *et al.*, 2004), which does not justify the up to ~9000 ppm measured in our xenoliths. Therefore, the enrichment in F and B, and possibly of other elements as As, with respect to both volcanic products and carbonate, may be related to their incompatible behaviour with respect to the magma and their partitioning into the gas phase of the eruption cloud.

The temperatures derived from isotope modelling agree with the stability condition of fluoborite and humite found in our xenoliths and strongly suggests that metasomatism of carbonates started contemporaneously with the circulation and release of fluids, with the zeolitization process starting afterwards.

Conclusions

The mineralogy, paragenesis and stable isotope geochemistry of xenoliths served as a basis to investigate the physico-chemical conditions during the Campanian Ignimbrite emplacement at the Fiano site (~50 km from the eruption source). The data of the present study, together with literature data, indicate infiltration of a fluid enriched in F, B, Mg and As through dominantly water-rich fluids affecting the carbonate rocks starting from temperatures of ~300–450°C.

A suggestion for possible future investigations is modelling and quantitative evaluations of the environmental impact of hazardous elements. Flourine, As and B have been immobilized by metamorphic reactions in the Fiano nodules. Further studies should quantify the possible local release and concentrations of F, As and B in soils, groundwater and atmosphere, with implications on the environmental impact of the eruption.

Acknowledgements

G. Balassone wishes to dedicate this work to the memory of Enrico Franco, inspiring Mineralogist and academic Teacher at the University of Naples (Italy). The reviews of Ştefan Marincea and Gianluca Iezzi and the comments of Roger Mitchell and Pete Leverett helped to improve the quality of the paper. Financial support to this research came from University of Naples 2014 fund granted to G.B. and from the COFIN MIUR 2010-2011 (2010EARRRZ_010) granted to University of Bari. Dr. R. de Gennaro (DiSTAR, University of Naples) is thanked for help with SEM-EDS analyses. V. Monetti and L.M. Francese (DiSTAR, University of Naples) assisted with laboratory support. Prof. Stefano Poli and Andrea Risplendente (University of Milan) are acknowledged for the facilities at the Electron Microprobe Laboratory. Facilities at the Centro Interdipartimentale Laboratorio di Ricerca per la Diagnostica dei Beni Culturali, University of Bari Aldo Moro, are also acknowledged.

References

Arienzo, I., Heumann, A., Wörner, G., Civetta, L. and Orsi, L. (2011) Processes and timescales of magma evolution prior to the Campanian Ignimbrite eruption (Campi Flegrei, Italy). *Earth and Planetary Science Letters*, **306** (3–4), 217–228.

Bachechi, F., Federico, M. and Fornaseri, M. (1966) La ludwigite e i minerali che l'accompagnano nelle geodi delle "pozzolane nere" di Corcolle (Tivoli, Colli Albani). *Periodico di Mineralogia*, **35**, 975–1022.

Balassone, G., Franco, E., Mattia, C.A., Petti, C. and Puliti, R. (2002) Re-examination of fluosiderite, an unknown mineral from southern Italy: equal to fluorine-rich chondrodite. *European Journal of Mineralogy*, **14**, 151–155.

Balassone, G., Scordari, F., Lacalamita, M., Schingaro, E., Mormone, A., Piochi, M., Petti, C. and Mondillo, N. (2013) Trioctahedral micas in xenolithic ejecta from recent volcanism of the Somma-Vesuvius (Italy): Crystal chemistry and genetic inferences. *Lithos*, **160–161**, 84–97.

Barberi, F. and Leoni, L. (1980) Metamorphic carbonate ejecta from Vesuvius Plinian eruptions: Evidence of the occurrence of shallow magma chambers. *Bullettin of Volcanology*, **43**, 107–120.

Betteridge, P.W., Carruthers, J.R., Cooper, R.I., Prout, K. and Watkin, D.J. (2003) Crystals version 12: software for guided crystal structure analysis. *Journal of Applied Crystallography*, **36**, 1487.

Bottinga, Y. (1968) Calculation of fractionation factors for carbon and oxygen isotopic exchange in the system calcite-carbon dioxide-water. *The Journal of Physical Chemistry*, **72**, 800–808.

Bowman, J.R. (1998) Stable-isotope systematics of skarns. Pp. 99–145 in: *Mineralized intrusion-related skarn systems* (D.R. Lentz, editor). Short Course Series, **26**. Mineralogical Association of Canada, Ottawa.

Brisi, C. and Eitel, W. (1957) Identity of nocerite and fluoborite. *American Mineralogist*, **42** (3–4), 288–293.

Bruker (2007). *SAINT*, Bruker AXS Inc., Madison, Wisconsin, USA.

https://doi.org/10.1180/minmag.2016.080.155 Published online by Cambridge University Press

Bruker (2009). *SADABS*, Bruker AXS Inc., Madison, Wisconsin, USA.

Cámara, F. and Ottolini, L. (2000) New data on the crystal-chemistry of fluoborite by means of SREF, SIMS, and EMP analysis. *American Mineralogist*, **85**, 103–107.

Caponera, I., Fiori, S. and Pucci, R. (2003) Fluoborite, piombo nativo, richterite ed altri interessanti ritrovamenti nei Colli Albani. Il Cercapietre. *Notiziario del Gruppo Mineralogico Romano*, **1–2**, 3–13.

Cappelletti, P., Cerri, G., Colella, A., de' Gennaro, M., Langella, A., Perrotta, A. and Scarpati, C. (2003) Post-eruptive processes in the Campanian Ignimbrite. *Mineralogy and Petrology*, **79**, 79–97.

Carati, M. (1987) I minerali degli inclusi metamorfosati nel tufo grigio campano. *Notiziario del Gruppo Mineralogico Geologico Napoletano*, **18**, 6–13.

Cesare, B., Cruciani, G. and Russo, U. (2003) Hydrogen deficiency in Ti-rich biotite from anatectic metapelites (El Joyazo, SE Spain): Crystal-chemical aspects and implications for high-temperature petrogenesis. *American Mineralogist*, **88**, 583–595.

Civetta, L., Orsi, G., Pappalardo, L., Fisher, R.V., Heiken, G. and Ort, M. (1997) Geochemical zoning, mingling, eruptive dynamics and depositional processes – the Campanian Ignimbrite, Campi Flegrei caldera, Italy. *Journal of Volcanology and Geothermal Research*, **75**, 183–219.

Costa, A., Folch, A., Macedonio, G., Giaccio, B., Isaia, R. and Smith, V.C. (2012) Quantifying volcanic ash dispersal and impact of the Campanian Ignimbrite super-eruption. *Geophysical Research Letters*, **39**, l–5.

de Gennaro, M., Calcaterra, D. and Langella, A. (2013) *Le pietre storiche della Campania – dall'oblio alla riscoperta*. Lucianoeditore, Napoli, Italy.

Della Ventura, G., Parodi, G.C. and Maras, A. (1992) Potassium-fluor-richterite, a new amphibole form San Vito, Monte Somma, Campania, Italy. *Rendiconti dell'Accademia dei Lincei, Classe di Scienze Fisiche, Maematiche e Naturali*, **9**, 239–245.

Del Moro, A., Fulignati, P., Marianelli, P. and Sbrana, A. (2001) Magma contamination by direct wall rock interaction, constraints from xenoliths from the walls of a carbonate-hosted magma chamber (Vesuvius 1944 eruption). *Journal of Volcanology and Geothermal Research*, **112**, 15–24.

Droop G.T.R. (1987) A general equation for estimating Fe^{3+} concentrations in ferromagnesian silicates and oxides from microprobe analysis, using stoichiometric criteria. *Mineralogical Magazine*, **51**, 431–437.

Fedele, F.G., Giaccio, B., Isaia, R. and Orsi, G. (2002) Ecosystem impact of the Campanian Ignimbrite eruption in Late Pleistocene Europe. *Quaternary Research*, **57**, 420–424.

Fedele, L., Tarzia, M., Belkin, H.E., De Vivo, B., Lima, A. and Lowenstern, J.B. (2006) Magmatic-hydrothermal fluid interaction and mineralization in alkali-syenite nodules from the Breccia Museo pyroclastic deposit, Naples, Italy. Pp. 125–161 in: *Volcanism in Campania Plain: Vesuvius, Campi Flegrei and Ignimbrites* (B. De Vivo, editor). Developments in Volcanology, **9**. Elsevier.

Fedele, L., Scarpati, C., Marvin, L., Melluso, L., Morra, V. Perrotta, A. and Ricci, G. (2008) The Breccia Museo formation, Campi Flegrei, southern Italy: geochronology, chemostratigraphy and relationship with the Campanian Ignimbrite eruption. *Bulletin of Volcanology*, **10**, 1189–1219.

Fisher, R. V., Orsi, G., Ort, M. and Heiken, G. (1993) Mobility of a large-volume pyroclastic flow-emplacement of the Campanian ignimbrite, Italy. *Journal of Volcanology and Geothermal Research*, **56**, 205–220.

Flamini, A., Graziani, G. and Pagliuca, G. (1979) Synthesis of the fluorine end member of the fluoborite series. *American Mineralogist*, **64**, 229–231.

Fulignati, P., Panichi, C., Sbrana, A., Caliro, S., Gioncada, A. and Del Moro, A. (2005) Skarn formation at the walls of the 79AD magma chamber of Vesuvius (Italy): Mineralogical and isotopic constraints. *Neues Jahrbuch für Mineralogie Abhandlungen*, **181**, 53–66.

Giaccio, B., Isaia, R., Fedele, F.G., Di Canzio, E., Hoffecker, J., Ronchitelli, A., Sinitsyn, A.A., Anikovich, M., Lisitsyn, S.N. and Popov, V.V. (2008) The Campanian Ignimbrite and Codola tephra layers: Two temporal/stratigraphic markers for the Early Upper Palaeolithic in southern Italy and eastern Europe. *Journal of Volcanology and Geothermal Research*, **177**, 208–226.

Gianfagna, A., Scordari, F., Mazziotti-Tagliani, S., Ventruti, G. and Ottolini, L. (2007) Fluorophlogopite from Biancavilla (Mt. Etna, Sicily, Italy): Crystal structure and crystal chemistry of a new F-dominant analog of phlogopite. *American Mineralogist*, **92**, 1601–1609.

Gilg, H.A., Lima, A., Somma, R., Belkin, H.E., De Vivo, B. and Ayuso, R.A. (2001) Isotope geochemistry and fluid inclusion study of skarns from Vesuvius. *Mineralogy and Petrology*, **73**, 145–176.

Hawthorne, F.C., Oberti, R., Harlow, G.E., Maresch, W.V., Martin, R.F., Schumacer, J.C., Welch, M.D. (2012) Nomenclature of the amphibole supergroup. *American Mineralogist*, **97**, 2031–2048.

Hazen, R.M. and Burnham, C.W. (1973) The crystal structures of one-layer phlogopite and annite. *American Mineralogist*, **58**, 889–900.

Hazen, R.M., Finger, L.W. and Velde, D. (1981) Crystal structure of a silica- and alkali-rich trioctahedral mica. *American Mineralogist*, **66**, 586–591.

Heinrich, W. (1994) Potassium-fluor-richterite in meta-cherts from the Bufa del Diente contact-metamorphic aureole, NE-Mexico. *Mineralogy and Petrology*, **50**, 259–270.

Iannace, A. (1991) Ambienti deposizionali e processi diagenetici in successioni di piattaforma carbonatica

https://doi.org/10.1180/minmag.2016.080.155 Published online by Cambridge University Press

del Trias Superiore nei Monti Lattari e Picentini (Salerno). PhD Thesis, Università di Napoli "Federico II", Naples, Italy.

Joswig, V.W. (1972) Neutronenbeugungsmessungen an einem 1*M*-Phlogopit. *Neues Jahrbuch für Mineralogie, Monatshefte*, 1–11.

Langella, A., Bish, D.L., Cappelletti, P., Cerri, G., Colella, A., de Gennaro, R., Graziano, S.F., Perrotta, A., Scarpati, C. and de Gennaro, M. (2013) New insights into the mineralogical facies distribution of Campanian Ignimbrite, a relevant Italian industrial material. *Applied Clay Science*, **72**, 55–73.

Leeman, W.P., Sisson, V.B. and Reid, M.R. (1992) Boron geochemistry of the lower crust: evidence from granulite terranes and deep crustal xenoliths. *Geochimica et Cosmochimica Acta*, **56**, 775–788.

Marianelli, P., Sbrana, A. and Proto, M. (2006) Magma chamber of the Campi Flegrei supervolcano at the time of eruption of the Campanian Ignimbrite. *Geology*, **34**, 937–940.

Marincea, Ş. (2000) Fluoborite in magnesian skarns from Baita Bihor (Bihor Massif, Apuseni Mountains, Romania). *Neues Jahrbuch für Mineralogie, Monatshefte*, **8**, 357–371.

Masi, U. and Turi, B. (1972) Frazionamento isotopico del carbonio e dell'ossigeno negli inclusi calcarei metamorfosati del "Tufo grigio campano" Auct. di Fiano (Salerno). *Periodico di Mineralogia*, **41**, 291–310.

McCauley, J.W., Newnham, R.E. and Gibbs, G.V. (1973) Crystal structure analysis of synthetic fluorophlogopite. *American Mineralogist*, **58**, 249–254.

McDonough, W.F. and Sun, S.S. (1995) The composition of the Earth. *Chemical Geology*, **120**, 223–253.

Ort, M.H, Rosi, M. and Anderson, C.D. (1999) Correlation of deposits and vent locations of the proximal Campanian Ignimbrite deposits, Campi Flegrei, Italy, based on natural remanent magnetization and anisotropy of magnetic susceptibility characteristics. *Journal of Volcanology and Geothermal Research*, **91**, 167–178.

Ottolini, L., Schingaro, E. and Scordari, F. (2012) Ceramics: Contribution of Secondary Ion Mass Spectrometry (SIMS) to the Study of Crystal Chemistry of Mica Minerals. Pp. 1017–1060 in: *Mass Spectrometry Handbook*. Wiley Series on Pharmaceutical Science and Bioteechnology: Practices, Applications, and Methods, **43**. J. Wiley & Sons, Hoboken, NJ, USA.

Pappalardo, L., Ottolini, L. and Mastrolorenzo, G. (2008) The Campanian Ignimbrite (southern Italy) geochemical zoning: insight on the generation of a supereruption from catastrophic differentiation and fast withdrawal. *Contribution to Mineralogy and Petrology*, **156**, 1–26.

Piochi, M., Bruno, P.P. and De Astis, G. (2005) Relative roles of rifting tectonics and magma ascent processes: inferences from geophysical, structural, volcanological, and geochemical data of the Neapolitan volcanic region (southern Italy). *Geochemistry, Geophysics, Geosystems*, **6**, 1–25.

Piochi, M., Polacci, M., De Astis, G., Zanetti, A., Mangiacapra, A., Vannucci, R. and Giordano, D. (2008) Texture and composition of pumices and scoriae from the Campi Flegrei caldera (Italy): Implications on the dynamics of explosive eruptions. *Geochemistry Geophysics Geosystems*, **9**, 1–25.

Piochi, M., Mormone, A., Balassone, G., Strauss, H., Troise, C. and De Natale, G. (2015) Native sulfur, sulfates and sulfides from the active Campi Flegrei volcano (southern Italy): Genetic environments and degassing dynamics revealed by mineralogy and isotope geochemistry. *Journal of Volcanology and Geothermal Research*, **304**, 180–193.

Polacci, M., Pioli, L. and Rosi, M. (2003) The Plinian phase of the Campanian Ignimbrite eruption (Phlegrean Fields, Italy): evidence from density measurements and textural characterization of pumice. *Bulletin of Volcanology*, **65**, 418–432.

Redhammer, G.J. and Roth, G. (2002) Single-crystal structure refinements and crystal chemistry of synthetic trioctahedral micas $KM_3(Al^{3+}, Si^{4+})_4O_{10}(OH)_2$, where M = Ni^{2+}, Mg^{2+}, Co^{2+}, Fe^{2+}, or Al^{3+}. *American Mineralogist*, **87**, 1464–1476.

Rosen, O., Desmons, J. and Fettes, D. (2007) *A systematic nomenclature for metamorphic rocks. 7. Metacarbonates and related rocks*. Recommendations by the IUGS Subcommission on the systematics of metamorphic rocks. SCMR website (www.bgs.ac.uk/SCMR).

Russell, R.L. and Guggenheim, S. (1999) Crystal structures of near-end-member phlogopite at high temperatures and heat-treated Fe-rich phlogopite; the influence of the O, OH, F site. *The Canadian Mineralogist*, **37**, 711–720.

Scacchi, A. (1888) La regione vulcanica fluorifera della Campania. *Atti della Reale Accademia delle Scienze Fisiche e Matematiche di Napoli*, **2**, 1–108.

Scacchi, A. (1890) La regione vulcanica fluorifera della Campania. *Memorie Regio Comitato Geologico Italiano, Estratti*, **IV**(I), 1–48.

Schingaro, E., Lacalamita, M., Scordari, F., Brigatti, M.F. and Pedrazzi, G., (2011) Crystal chemistry of Ti-rich fluorophlogopite from Presidente Olegario, Alto Paranaíba igneous province, Brazil. *American Mineralogist*, **96**, 732–743.

Schingaro, E., Lacalamita, M., Scordari, F. and Mesto, E. (2013) 3*T*-phlogopite from Kasenyi kamafugite (SW Uganda): EPMA, XPS, FTIR, and SCXRD study. *American Mineralogist*, **98**, 709–717.

Schingaro, E., Kullerud, K., Lacalamita, M., Mesto, E., Scordari, F., Zozulya, D., Erambert, M. and Ravna, E. J.K. (2014) Yangzhumingite and phlogopite from the

https://doi.org/10.1180/minmag.2016.080.155 Published online by Cambridge University Press

Kvaløya lamproite (North Norway): Structure, composition and origin. *Lithos*, **210–211**, 1–13.

Scordari, F., Schingaro, E., Ventruti, G., Nicotra, E., Viccaro, M. and Mazziotti Tagliani, S. (2013) Fluorophlogopite from Piano delle Concazze (Mt. Etna, Italy): crystal chemistry and implications for the crystallization conditions. *American Mineralogist*, **98**, 1017–1025.

Shannon, R.D. (1976) Revised effective ionic radii and systematic studies of interatomic distances in halides and chalcogenides. *Acta Crystallogaphica*, **A32**, 751–767.

Signorelli, S., Vaggelli, G., Romano, C. and Carroll, M.R. (2001) Volatile element zonation in Campanian Ignimbrite magmas (Phlegrean Fields, Italy): evidence from the study of glass inclusions and matrix glasses. *Contribution to Mineralogy and Petrology*, **140**, 543–553.

Takeda, H. and Donnay, J.D.H. (1966) Trioctahedral One-Layer Micas. III. Crystal Structure of a Synthetic Lithium Fluormica. *Acta Crystallographica*, **A20**, 638–646.

Takeda, H. and Morosin, B. (1975) Comparison of observed and predicted structural parameters of mica at high temperature. *Acta Crystallographica*, **B31**, 2444–2452.

Taylor, H.P., Giannetti, B and Turi, B (1979) Oxygen isotope geochemistry of the potassic igneous rocks from the Roccamonfina volcano, Roman comagmatic region, Italy. *Earth and Planetary Science Letters*, **46**, 81–106.

Tell, I. (1974) Hydrothermal Studies on Fluorine Metamorphic Reactions in Siliceous Dolomite. *Contribution to Mineralogy and Petrology*, **43**, 99–110.

Tomlinson, E.L., Arienzo, I., Civetta, L., Wulf, S., Smith, V.C., Hardiman, M., Lane, C.S., Carandente, A., Orsi, G., Rosi, M., Müller, W. and Menzies, M.A. (2012) Geochemistry of the Phlegraean Fields (Italy) proximal sources for major Mediterranean tephras: Implications for the dispersal of Plinian and co-ignimbritic components of explosive eruptions. *Geochimica et Cosmochimica Acta*, **93**, 102–128.

Tonarini, S., Leeman, W.P., Civetta, L., D'Antonio, M., Ferrara, G. and Necco, A. (2004) B/Nb and $\delta^{11}B$ systematics in the Phlegrean Volcanic District, Italy. *Journal of Volcanology and Geothermal Research*, **133**, 123–139.

Turi, B. (1969) Carbon and oxygen isotopic composition of carbonates in limestones blocks and related geodes from the "Black Pozzolans" formation of the Alban Hills. *Chemical Geology*, **5**, 195–205.

Vitale, S. and Isaia, R. (2014) Fractures and faults in volcanic rocks (Campi Flegrei, southern Italy): insight into volcano-tectonic processes. *International Journal of Earth Sciences*, **103**, 801–819.

Weiss, Z., Rieder, M. and Chmielová, M. (1992) Deformation of coordination polyhedra and their sheets in phyllosilicates. *European Journal of Mineralogy*, **4**, 665–682.

White, J.S. (1981) Grothine discredited, equals norbergite. *The Mineralogical Record*, **12**, 377–378.

Whitney, D.L. and Evans B.W. (2010) Abbreviations for names of rock-forming minerals. *American Mineralogist*, **95**, 185–187.

Zambonini, F. (1919) Il tufo pipernoide della Campania e i suoi minerali. *Memorie per servire alla Descrizione della Carta Geologica d'Italia*, **7**, pp. 130.

Zheng, Y.F. (1990) Carbon-oxygen isotopic covariation in hydrothermal calcite during degassing of CO_2. A quantitative evaluation and application to the Kushikino gold mining area in Japan. *Mineralium Deposita*, **25**, 246–250.

Zheng, Y.F. and Hoefs, J. (1993) Carbon and oxygen isotope covariations in hydrothermal calcites. *Mineralium Deposita*, **28**, 79–89.

https://doi.org/10.1180/minmag.2016.080.155 Published online by Cambridge University Press